New Differential Zone Protection Scheme Using Graph Partitioning for an Islanded Microgrid

Fahad S. Alsaeidi

Thesis submitted to the Faculty of the
Virginia Polytechnic Institute and State University
in partial fulfillment of the requirements for the degree of

Master of Science
in
Electrical Engineering

Chen-Ching Liu, Chair
Jaime De La Ree
Ali Mehrizi-Sani

April 20, 2022
Blacksburg, Virginia

Keywords: Microgrid, Microgrid Protection, Differential Protection, Graph Theory, Graph Partitioning Algorithm

New Differential Zone Protection Scheme Using Graph Partitioning for an Islanded Microgrid

Fahad S. Alsaeidi

(ABSTRACT)

Microgrid deployment in electric grids improves reliability, efficiency, and quality, as well as the overall sustainability and resiliency of the grid. Specifically, microgrids alleviate the effects of power outages. However, microgrid implementations impose additional challenges on power systems. Microgrid protection is one of the technical challenges implicit in the deployment of microgrids. These challenges occur as a result of the unique properties of microgrid networks in comparison to traditional electrical networks. Differential protection is a fast, selective, and sensitive technique. Additionally, it offers a viable solution to microgrid protection concerns. The differential zone protection scheme is a cost-effective variant of differential protection. To implement a differential zone protection scheme, the network must be split into different protection zones. The reliability of this protection scheme is dependent upon the number of protective zones developed. This thesis proposes a new differential zone protection scheme using a graph partitioning algorithm. A graph partitioning algorithm is used to partition the microgrid into multiple protective zones. The IEEE 13-node microgrid is used to demonstrate the proposed protection scheme. The protection scheme is validated with MATLAB Simulink, and its impact is simulated with DIgSILENT PowerFactory software. Additionally, a comprehensive comparison was made to a comparable differential zone protection scheme.

New Differential Zone Protection Scheme Using Graph Partitioning for an Islanded Microgrid

Fahad S. Alsaeidi

(GENERAL AUDIENCE ABSTRACT)

A microgrid is a group of connected distributed energy resources (DERs) with the loads to be served that acts as a local electrical network. In electric grids, microgrid implementation enhances grid reliability, efficiency, and quality, as well as the system's overall sustainability and resiliency. Microgrids mitigate the consequences of power disruptions. Microgrid solutions, on the other hand, bring extra obstacles to power systems. One of the technological issues inherent in the implementation of microgrids is microgrid protection. These difficulties arise as a result of microgrid networks' distinct characteristics as compared to standard electrical networks. Differential protection is a technique that is fast, selective, and sensitive. It also provides a feasible solution to microgrid protection problems. This protection scheme, on the other hand, is more expensive than others. The differential zone protection scheme is a cost-effective variation of differential protection that lowers protection scheme expenses while improving system reliability. The network must be divided into different protection zones in order to deploy a differential zone protection scheme. The number of protective zones generated determines the reliability of this protection method. Using a network partitioning technique, this thesis presents a new differential zone protection scheme. The microgrid is divided into various protection zones using a graph partitioning algorithm. The proposed protection scheme is demonstrated using the IEEE 13-node microgrid. MATLAB Simulink is used to validate the protection scheme, while DIgSILENT PowerFactory is used to simulate its impact. A comparison of a similar differential zone protection scheme was also done.

Dedication

To my cherished homeland of Kuwait,

to my mother, and to my family

Acknowledgments

In the name of Allah, the Most Gracious and the Most Merciful. All praise to Allah and His blessings for the completion of this thesis. I thank God For the opportunity, trails, and fortitude to accomplish the thesis. My sincere gratitude to the holy Prophet Muhammad (Peace be upon him), whose way of life has served as a constant guide for me.

I am really appreciative to Dr. Chen-Ching Liu, my adviser, for his instruction, encouragement, and patience. This effort would not have been feasible without his guidance and motivation. I would like to thank Drs. Jaime De La Ree and Ali Mehrizi-Sani for being on my committee.

Additionally, I would like to express my heartfelt appreciation to the Bradley Department of Electrical and Computer Engineering and Virginia Tech for the opportunity to study as a graduate student. Additionally, I want to express my gratitude to all of my instructors at Virginia Tech. I gained a great amount of knowledge from them. This work would be impossible to complete without their direction and assistance. Additionally, I want to express my gratitude to my colleagues and friends at the Power and Energy Center for their assistance and encouragement.

Additionally, I am grateful to my home country, Kuwait, and my employer, the public authority for applied education and training (PAAET), for their generous scholarship. Additionally, I'd want to express my gratitude to the Kuwaiti embassy in Washington, DC, and the Kuwait cultural attache for their assistance and support.

Finally, I want to extend my gratefulness and gratitude to my family, both here in the United States and in Kuwait. I could not have achieved this work without their unwavering support and prayers.

Contents

List of Figures

List of Tables

Chapter 1

Introduction

1.1 Motivation

Microgrids provide several advantages and benefits to power utilities and communities. Microgrids enhance the reliability, efficiency, and quality of electric service, as well as the overall sustainability and resiliency of the electric grid. Additionally, microgrids mitigate the damage that can be caused by extended power outages [1]. While microgrids provide several benefits, adopting them introduces a slew of new hurdles and challenges. Microgrid protection is one of these difficulties. Microgrid protection is difficult due to the microgrid's unique characteristics in comparison to traditional electric networks. Traditional electric distribution networks are radial in design, with a high fault current level, unidirectional power flow, and a single source of supply. While microgrids are meshed networks, they may have varying fault current levels depending on their operating mode, bidirectional power flow, and numerous distributed energy resources (DERs) [2, 3, 4, 5]. The need for a new protection scheme is important to address microgrid protection concerns while keeping costs in consideration.

1.2 Microgrids

A microgrid is a group of connected distributed energy resources (DERs) and the loads to be served that acts as a local electrical network [1, 6, 7, 8, 9, 10, 11]. There are several definitions of microgrids in the literature. The most often used definitions were provided by the United States Department of Energy (DOE) and the Conseil International des Grands Réseaux Electriques (CIGRE).

Microgrids are defined by the US Department of Energy (DOE) as "a group of interconnected loads and distributed energy resources within clearly defined electrical boundaries that act as a single controllable entity with respect to the grid. A microgrid can connect and disconnect from the grid to enable it to operate in both grid-connected or island-mode. "[12]

Microgrids, on the other hand, are defined by the CIGRE working group C6.22, Microgrid Evolution Roadmap, as "microgrids are electricity distribution systems containing loads and distributed energy resources, (such as distributed generators, storage devices, or controllable loads) that can be operated in a controlled, coordinated way either while connected to the main power network or while islanded."[13]

As illustrated by the two definitions above, the primary criteria for a microgrid are that it connects loads and DERs in a controlled and safe manner, with clearly defined boundaries, and that it supports both grid-connected and islanding operation.

Microgrid development and adoption in places with existing electrical grid infrastructure are being driven by three key factors: energy security, economic benefits, and clean energy integration [14]. One of the primary reasons for microgrid development, particularly in the United States, is the capacity of microgrids to improve the electric power grid's reliability and resiliency. When the major grid is down due to severe weather or cascading events, microgrids can supply critical facilities and communities by utilizing their distributed energy

resources (DERs) [15, 16, 17, 18].

While these benefits are substantial for any electric network, implementing a microgrid presents significant challenges. The microgrid's most common issues have been classified into four categories: Technical difficulties, regulatory difficulties, financial difficulties, and stakeholder difficulties [1]. The technical obstacles associated with microgrids are technological, dual-mode operation, power quality, and protection [1, 9, 11, 14]. This thesis examines the issues associated with microgrid protection and how to address them.

1.3 Microgrid Protection

Microgrids are small electrical networks that require protection in order to de-energize and isolate faults before they cause damage or harm to people or property. By isolating and mitigating disturbances, protection systems ensure the continued operation of vital infrastructure [19]. The protection of traditional distribution systems is based on the assumption that the system is fed from a single source and has a radial topology. Microgrids, on the other hand, maybe fed from a variety of distributed sources, altering the direction and magnitude of fault currents accordingly. Microgrid protection is a critical concern in islanded operations [2, 3, 4, 5, 20, 21]. Due to the high penetration of inverter-based resources (IBRs), the fault currents in a grid-connected and an islanded microgrid are considerably different. IBRs lead to fault currents that are difficult to detect or isolate using a conventional protection schemes.

1.3.1 Microgrid Protection Challenges

Microgrid deployments pose additional control, operation, and protection challenges. Microgrid protection issues develop when a microgrid has many DERs. Additionally, IBRs penetration complicates microgrid protection by introducing new issues, such as restricted fault current contribution. Furthermore, various operation modes present new challenges, such as varying fault current levels in each mode. The following are the primary protection challenges that arise in microgrid protection:

- **Bidirectional flow of current:** Traditional distribution networks are radial in nature and fed from a single source (a substation feeder). Typically, such networks are protected using the conventional overcurrent protection scheme. However, since microgrids have many power sources, the power flow will be bidirectional. In this instance, traditional overcurrent protection is incapable of detecting and isolating faults appropriately [2, 3, 5, 21, 22].

- **Variable fault current level:** Due to the microgrid's dual operating mode, the fault current level varies significantly between modes. The fault current level is high in grid-connected mode. On the other hand, when the microgrid is operated in an islanded mode, the fault current level is drastically decreased. Developing a protection scheme that is effective in all modes of operation is challenging [2, 3, 5, 21, 22].

- **Limited fault current produced by IBRs:** A current limiter regulates the IBR's current to prevent overcurrent damage to the semiconductor switching devices. IBRs restrict the amount of fault current they contribute to 1.1–1.5 pu of the inverter's nominal current rating [2]. Due to the difficulty of distinguishing fault current from overload current at this low fault current level, conventional protection schemes may fail to identify such fault current [2, 3, 5, 21].

- **Protection blinding:** Each DER contributes to the fault current as a result of its incorporation into microgrids. Thus, the magnitude of the fault current will be dispersed and reduced throughout the microgrid. This reduces the speed and sensitivity of the upstream protection devices [3, 22].

- **Sympathetic tripping:** Sympathetic tripping occurs when a protective relay responds to a fault outside of its protection zone. This unintended tripping results in an outage of the unfaulty zones [3, 22].

1.3.2 Microgrid Protection Solutions

One of the earliest microgrid protection schemes [20] was proposed by Nikkhajoei and Lasseter. This protection scheme is based on symmetrical components and residual current measurements. To detect faults in this scheme, a differential current equal to the sum of the three phase currents and the neutral current is utilized. This approach is capable of detecting asymmetrical faults located upstream of the protected zone. Additionally, this design includes two backup protections: I^2t protection as the primary backup and under-voltage protection as the secondary backup.

Numerous microgrid protection schemes have been proposed recently [5, 22, 23, 24, 25]. These protection schemes are categorized in the literature according to their core concepts. Microgrid protection schemes may be classified into four broad categories: adaptive, differential, traveling wave, and other protection schemes [22].

- **Adaptive-based protection schemes:** The adaptive protection schemes automatically adjust the relay setting based on the microgrid status. Off-line adaptive protection [26, 27, 28] and on-line adaptive protection [29, 30] are two main categories of adaptive protection schemes. Off-line adaptive protection stores microgrid data and

relay settings for each operation scenario. While in the online adaptive protection, the relay setting is dynamically adjusted in response to real-time system data.

- **Differential-based protection schemes:** Differential protection is a frequently utilized approach for microgrid protection. Current differential protection is unaffected by variations in fault current, bidirectional current flow, the state of DERs, or changes in system configuration [22]. Numerous differential protection systems can be found in the literature [31, 32, 33]. The differential protection schemes are extremely fast, selective, and sensitive. On the other hand, the key drawback of this protective approach is its enormous expense. E. Sortomme et al. presented a differential zone protection scheme to lower the cost of differential protection [34]. In this scheme, the microgrid is divided into small protective zones. The total of all entering current and outgoing current should be zero in each protective zone. The differential current in each protective zone is defined as the total of all incoming and outgoing currents. The protection zones are selected using a genetic algorithm that minimizes the cost of the protection devices and the cost of customer interruption over a ten-year period. In this scheme, each protective zone is assumed to have a generation and load balance. While this technique works well when the microgrid is connected to the grid, it does not ensure the continuous functioning of an islanded microgrid.

- **Traveling wave based protection schemes:** The traveling wave approach has been widely employed in high voltage transmission systems, particularly in HVDC systems, for fault detection. However, due to limiting issues such as high sampling frequency, noise disruption, and so on [35], it is rarely employed to protect microgrids. In [36], A fault detection technique based on traveling waves is developed for inverter-dominated microgrids. Improved mathematical morphology (MM) is used in this paper to capture the polarity of an initial current traveling wave.

- **Other protection schemes:** Other protection schemes such as voltage-based protection, total harmonic distortion THD-based protection, and phasor-based protection are present in the literature. [37] proposes a voltage-based protection scheme that detects faults by monitoring voltage disturbances in the q-axis. [38] describes a protection scheme based on total harmonic distortion THD. By monitoring the voltage at the fundamental frequency and THD of each phase, the type and location of the fault can be determined using this approach. [39] proposes a phasor-based protection scheme. The fault is identified in this technique by analyzing the fault current's symmetrical components and the phase differences between the main and branch feeders.

1.4 Thesis Contributions

The literature has a few differential zone protection schemes. One of the best known differential zone protection schemes was devised by Sortomme et al.[34]. A genetic algorithm is utilized in this scheme to reduce the cost of the protection system. While this is an innovative and exciting solution, it cannot guarantee the entire operation of microgrids in islanded mode since it does not ensure that each protection zone has an adequate generation and load balance.

This thesis proposes a new differential zone protection scheme using a graph partitioning algorithm. By utilizing the graph partitioning algorithm in [40], the microgrid will be split into different protective zones. This graph partitioning algorithm balances the generation-to-load ratio in each protection zone to the maximum extent possible. Additionally, the proposed protection scheme ensures that each protection zone has an acceptable generation and load balance. Only the affected zone will be isolated during

faults; the remaining zones will function as a single large zone with appropriate generation and load balance.

1.5 Thesis Outline

The remaining of this thesis is composed of the following: Chapter 2 presents the proposed protection scheme. Chapter 3 illustrates the proposed protection scheme simulation. Chapter 4 compares the proposed differential zone protection scheme with the differential zone protection scheme in [34]. Finally, Chapter 5 contains the conclusion and suggestions for further research.

Chapter 2

Proposed Protection Scheme

2.1 Introduction

The differential protection scheme is based on the differential comparison concept, which is among the most sensitive and effective techniques for protecting the power system from internal faults [19]. Differential protection is a simple and straightforward process. For instance, differential current protection compares the currents entering and exiting the equipment. The two currents are equal in normal operation, and the difference between them should be zero; nevertheless, in abnormal conditions, particularly when a fault occurs between the two terminals, the difference between the two currents will not be zero. If the differential current exceeds the threshold limits in this instance, the protective device (relay) will detect the fault and isolate the equipment or protected devices.

The differential current protection principle is illustrated in Figure 2.1. Under normal circumstances, the current entering the equipment should equal the current leaving it; in this example, the entering current is I_1, and the leaving current is I_2. Current transformers are used to reduce the power current to an acceptable level for the protective relays, which are typically between 1A and 5A, depending on the relay's specifications. The dot convention in the CT is meant to create an opposition between the two currents. While the differential current $i_{diff} = i_1 - i_2$ is zero during normal operation, it is not zero during fault incidence. The differential current flows through the relay coil, and then a trip signal is delivered to

the circuit breaker, thereby isolating the equipment.

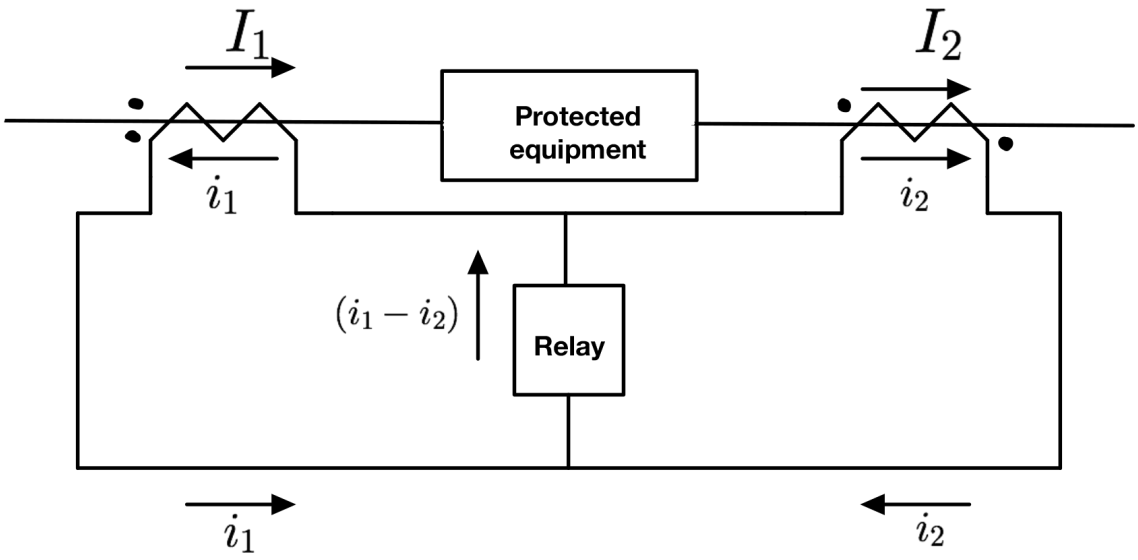

Figure 2.1: Current Differential Comparison Principle.

Differential protection is a potential approach to addressing the microgrid protection challenges [2, 3, 4, 5, 10, 21, 41]. Additionally, differential protection may improve the resiliency and reliability of the microgrid. Differential protection has been a commonly used method for microgrid protection. Dewadasa et al.[32] proposed differential relay-based protection methods for microgrids. On the other hand, Sortomme et al.[31] developed a differential protection scheme with digital relays and a communication network that utilizes current differential protection as the primary protection. Additionally, Ustun et al.[33] proposed a communication-assisted differential current protection system. The primary downside of current differential protection is its high cost; this scheme demands that a relay be installed at each end of the microgrid line segments. To maximize the benefits of this protection strategy while reducing the expense, new improved differential protection is required.

2.2 Differential Zone Protection

As discussed previously, differential current protection is based on the comparison of two currents. This approach could be extended to compare several currents if their summing equals zero. Consider the IEEE 9-node network depicted in Figure 2.2.

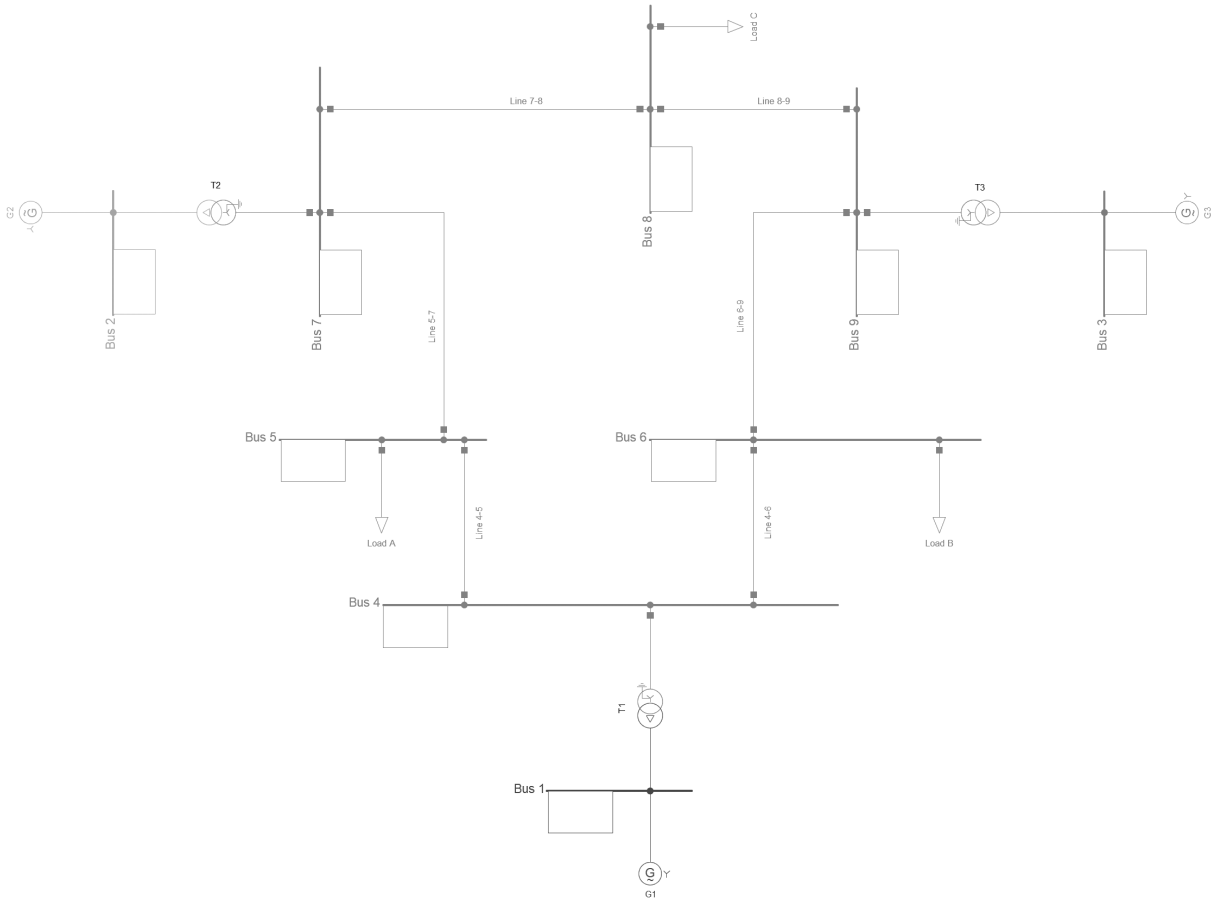

Figure 2.2: IEEE 9-node network.

The IEEE 9-node network can be simplified to a 6-node network by eliminating buses 1, 2, and 3. Due to the fact that this protection system requires just the measurement of the network's input and output currents, the transformer secondary currents are treated as generator currents, which equal the network's input current. The simplified 6-node network

depicted in Figure 2.3 is an illustration.

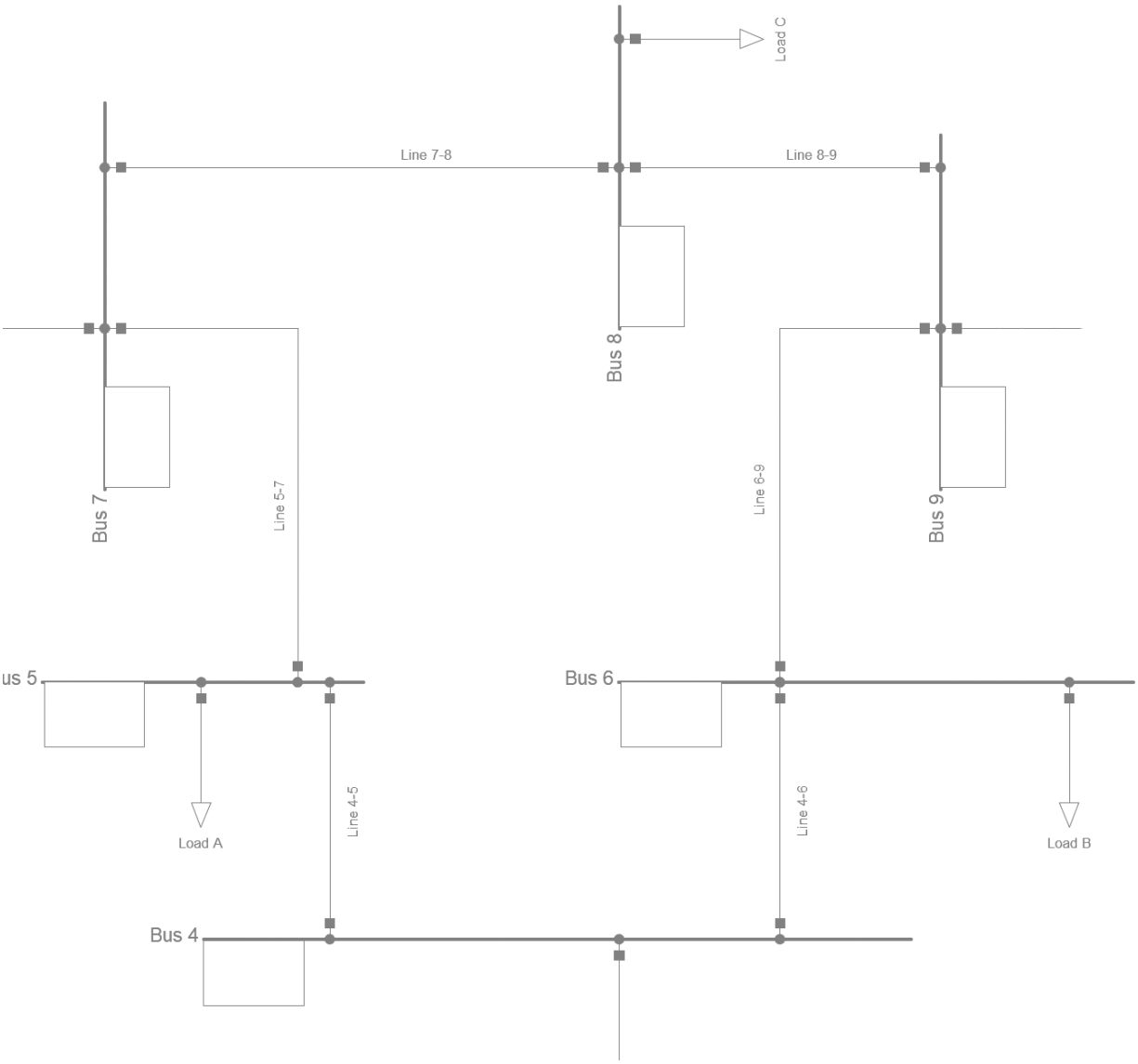

Figure 2.3: Simplified 6-node Network.

Three generators supply power to the network, and three loads consume it. The three generators' currents are denoted by the I_{G1}, I_{G2}, and I_{G3}, whereas I_{L1}, I_{L2}, and I_{L3} denote the three loads' currents. In a normal power system operating condition, the sum of the generators' currents flowing through the network should match the sum of the loads' currents.

While the majority of microgrid applications occur in distribution networks, capacitive leakage current is thought to be negligible. The differential current I_{diff} of the relay should be equal to $I_{diff} = \sum I_G - \sum I_L$ in this scenario. The differential current should be zero during normal operation. On the other hand, if any failures occur in the network, the differential current will exceed zero.

The differential zone protection scheme necessitates the installation of a protective relay at each network source and load. As explained later in this chapter, the load relays could be replaced by smart current sensors capable of measuring current phasors. The reason for replacing load relays with smart current sensors is that current interruption at the load is not essential to isolate the network. The three relays located at each source end will prohibit the sources from supplying any power to the network, thus isolating it.

2.3 Graph Partitioning Algorithm

Electric power networks may be represented using graph theory. Any network can be expressed in graph theory by a graph G, which consists of a pair of vertices set V and edges set E. Any electric network can be represented in power system applications by an undirected edge-weighted graph $G = (V, E)$, where a_{uv} is the edge weight assigned to each pair of vertices (u, v).

The adjacency matrix, the degree matrix, and the Laplacian matrix all characterize the graph G algebraically. The adjacency matrix A is a matrix containing the graph G's edge-weight element, where $A = [a_{uv}]$. The degree matrix D is a diagonal matrix containing the degree of each vertex, denoted by the symbol d_{vv} .The vertex degree is equal to the number of edges that connected to the vertex v. The Laplacian matrix Q is calculated by subtracting the

adjacency matrix A from the degree matrix D, as indicated in 2.1.

$$Q = D - A \tag{2.1}$$

The Laplacian matrix is defined in detail in [42].

Graph partitioning techniques have been used for applications in electric power systems. In [40, 43, 44, 45], the electric network is reconfigured following significant disturbances using graph partitioning approaches. Another use of graph partitioning techniques is optimal microgrid topology planning (MTP) [46, 47].

The implementation of the differential zone protection scheme requires that electric network to be divided into small protection zones. A graph partitioning approach is an effective method for dividing an electric network. Li et al.[40] developed a graph partitioning algorithm for splitting the electric grid into K islands in order to minimize generation and load imbalance. The electric network is transformed into a graph G using this approach; the network nodes serve as the graph G's vertices V, while the lines connecting the nodes serve as the graph G's edges E. This graph is an undirected edge-weighted graph, with the edge-weight a_{uv} equal to the absolute value of the real power flow in the lines.

In the proposed protection scheme, the graph partitioning algorithm described in [40] will be utilized to segment the microgrid into small protection zones. This algorithm for graph partitioning consists of five steps, which are detailed below:

Step 1: Convert the electric network to an edge-weighted graph G.

The electric network's power flow will be computed in this step. The electrical network is then transformed into an edge-weighted graph G. Each bus in the electric network is represented by a vertex V in the graph G, and each transmission line in the electric

network's single line diagram is denoted by an edge E in the graph G. Each edge in the graph G is assigned a weight based on the absolute value of the transmission line's real power flow.

Step 2: Compute the Laplacian matrix Q and its eigenvalues and their corresponding eigenvectors.

To compute the Laplacian matrix Q, the adjacency matrix A and the degree matrix D must be determined. As with equation 2.1, the Laplacian matrix is obtained by subtracting the adjacency matrix A from the degree matrix D. Then, the eigenvalues and their corresponding eigenvectors of the Laplacian matrix Q will be calculated. Therefore, the lowest eigenvalues $[\lambda_1, \lambda_2, ..., \lambda_k]$ and their corresponding eigenvectors $[x_1, x_2, ..., x_k]$ will be identified.

Step 3: Construct the partition vector from the first k eigenvectors of the Laplacian matrix Q.

The ratioed assignment matrix $X = [x_1, x_2, ..., x_k]$ is formed by the first k eigenvectors. The partition matrix $\widehat{P}$ can be recovered from a projecter of XX^T formed by the eigenvectors after normalization as indicated in Eq 2.2.

$$\widehat{P} = N(X)XX^TN(X) \tag{2.2}$$

where,

$N(X)$ is a diagonal matrix with $n_{ii} = 1/\sqrt{\sum_{h=1}^{k} x_{ih}'^2}$.

$X^T = [x_1', x_2', ..., x_k']$

n_{ii} is the reciprocal of the norm of row i of X.

Another approach in determining the partitioning matrix is indicated in Eq 2.3.

$$\widehat{P}_{ij} \quad = \quad x_i'^T x_j' / \left(\|x_i'\| \left\|x_j'\right\| \right) \tag{2.3}$$

$\widehat{P}_{ij}$ is the cosine of the angle between the two row vectors i, and j of X.

Step 4: Select k vertices to serve as the k seeds of the partitioned areas.

Let $Seeds = \{\}$ be a set of the seed vertices of the partitioned areas.

- First: choose any vertex in the graph as the first seed.

  then $Seeds = \{S_1\}$
- Second: find a new vertex v which satisfies $\{maxcos(v, S1)\}$ is minimized.
- Third: store the new seed into the vector seeds.

  $Seeds = \{Seeds\} \cup \{v\}$
- Finally: in the end the k seeds are selected. The vector seeds becomes

  $Seeds = \{S_1, S_2, ..., S_k\}$

Step 5: Classify the remaining $n - k$ vertices into the k areas and obtain the k partition.

Search the remaining vertices to classify them into the k partitioned areas. This search can be accomplished by finding the seeds $S_j, 1 \leq j \leq k$ that have the shortest distance to the vertex $v_i, 1 \leq i \leq n - k$.

This search can be done using the following method:

$for\ i = 1\ to\ (n - k)$

find the index j which $s.t\ cos(S_j, v_i)$ is maximized.

Let $P = \{A_1, A_2, ..., A_k\}$is the area set.

Then $A_j = A_j \cup \{v_i\}$

Now, the k-way partitions used to separate the electric power network into areas with the objective of minimizing the generation and load imbalance in each area have been obtained.

2.4 Proposed Protection Scheme

The differential zone protection scheme is a novel and creative approach for microgrid protection. Microgrids could be segmented into islands (protection zones), each with its own differential zone protection scheme. In the literature, there are only a few differential zone protection schemes for microgrids, Sortomme et al.[34] proposed a differential zone protection scheme. In this protection scheme, a genetic algorithm is used to minimize the investment cost of the protection devices and the cost of customer interruption over a ten-year period. Following optimization of relay placement, the microgrid will be partitioned into zones depending on relays locations. S. S. Venkata modified the optimization problem in [34] and substituted current measurements for real power measurements [5].

The previous differential zone protection scheme constructs protection zones through the use of a relay placement optimization algorithm. Due to the fact that this scheme does not ensure generation and load balance, it cannot be applied to an islanded microgrid. This scheme demands that the microgrid be connected to the grid in the event of a fault. The microgrid will be in grid-connected mode in order for it to have a generation and load balance. For instance, if a microgrid is divided into two zones and a fault develops in zone 1, the differential zone protection scheme isolates zone 1 while maintaining zone 2 energized. If zone 2 does not have sufficient generation to serve the loads, zone 2 will be turned off owing to generation shortages. As a result, the entire microgrid will be shut down, and the main purpose of this protection scheme is not achieved.

When operating in islanded mode, microgrid protection challenges arise. Any protection

scheme should operate satisfactorily in an islanded mode without the microgrid being connected to the utility grid. As a response, a new protection scheme is necessary.

This thesis proposed a new differential zone protection scheme. This protection scheme is comprised of two parts. The first part will develop a differential zone protection scheme for microgrids. Small zones will be formed within the microgrid. This system necessitates the use of digital relays, smart current sensors, and communication links. Digital relays will be installed on each source bus to measure the currents entering the protected zone, while smart current sensors will be installed at each load to measure the currents leaving the protected zone. The digital relays and smart current sensors should be capable of taking current phasor measurements, as the sum of all input and output currents will never equal zero unless the current measurements are in phasor form.

The second part of the proposed protection scheme is to divide the microgrid into small islands. Each island should have a generation and load balance. Maintaining a generation and load balance on each island is not simple; consequently, the ideal strategy is to minimize the generation and load imbalance. The most effective method for accomplishing this goal is through the application of graph theory and graph partitioning algorithms. The microgrid will be partitioned into small islands using the graph partitioning algorithm developed by Li et al.[40]. This partitioning algorithm is designed to minimize generating load imbalances.

The microgrid will be divided into small protection zones by employing the graph partitioning algorithm described in [40]. The segmentation of the microgrid will take place in stages. Divide the microgrid into two zones as a first stage. Zones A and B will be designated as the divided zones. The second stage is to determine whether the two split zones, A and B, may be further divided into two zones. The main condition for dividing zones is that they have more than one source of generation. Additionally, each divided zone should be capable of functioning independently of the main microgrid.

Each partitioned zone should be evaluated for its capability to be subdivided further. Each divided zone will undergo a zone feasibility test to determine whether these new zones can be further divided into new zones. Zone feasibility depends on the microgrid's topology and how unbalanced loads are distributed. The load on distribution networks is usually unbalanced. Microgrids are often used in distribution networks. The graph partitioning algorithm will keep splitting the microgrid until it achieves the unreliable condition of each DER having its own zone. To terminate the partitioning process, several constraints are necessary.

The microgrid is divided into small zones using graph partitioning. There might be a significant imbalance in these zones, or they could have only single-phase or two-phase networks. It is assumed that the DERs are three-phase. As a result of this circumstance, three-phase DERs may be used to serve a zone with only single-phase or two-phase power demands, which is not desirable. As a result, when this condition is fulfilled, the graph partitioning process will come to an end. On the other hand, to prevent the partitioned zones from overloading, the power transfer between the partitioned zones should not exceed 10% of the combined load of the two zones. Then, the partitioning process will be terminated, and the new zones will be rejected. In summary, every zone is considered feasible to be partitioned if the following requirements are met:

- Each zone should have an adequate balance between generation and load.

- Each zone contains three-phase power demand.

- The power transfer between the partitioned zones should not exceed 10% of the combined load of the two zones.

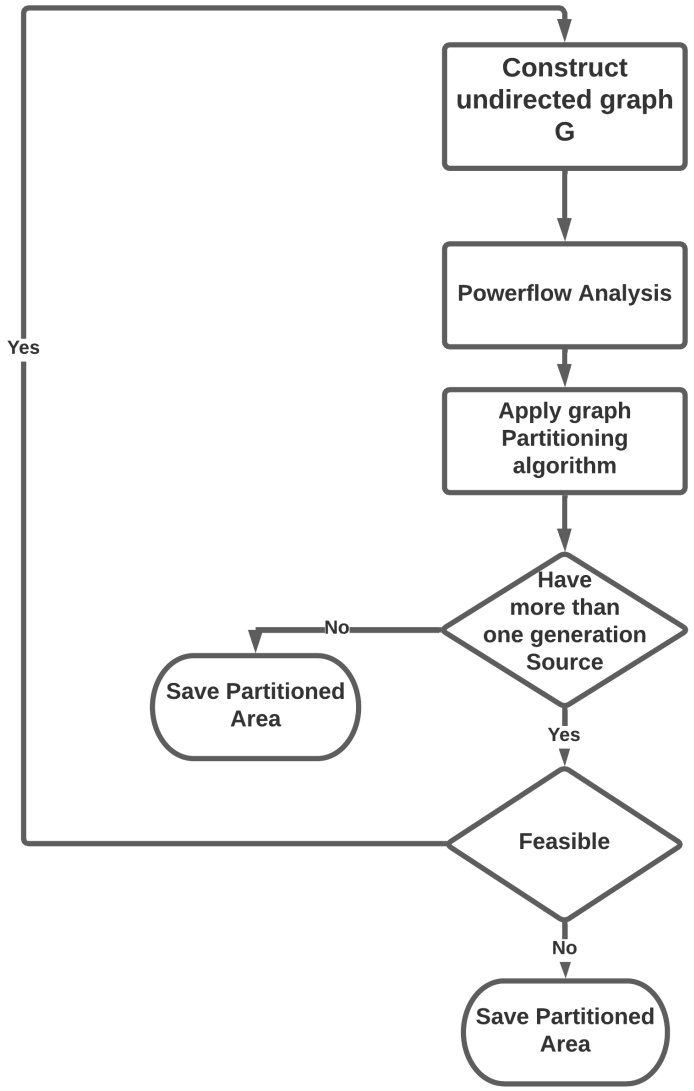

Figure 2.4: The Partitioning Process

The partitioning procedure is depicted in flow chart form in Figure 2.4. After partitioning the microgrid, each zone will be protected by the differential zone protection scheme separately. The total number of protective devices that will be used in this protection scheme is as follows:

- The number of digital relays utilized will be equal to the sum of the number of

generation sources and the number of created protection zones.

- The number of the smart current sensors will be equal to the total number of total loads.

A detailed simple example on how to implement the proposed protection scheme is illustrated in A.

2.5 Proposed Protection Scheme Feasibility

As previously stated in this chapter, the proposed protection scheme is only valid if three major components are present. Digital relays, smart current sensors, and communication links are the three components. Additionally, there is one condition that must be met in order for this protection scheme to be effective. This requirement can be satisfied through the use of digital relays and smart current sensors capable of performing phasor measurements. The differential zone protection scheme is based on the calculation of the sum of several currents. Unless the currents are in phasor quantities, the total of the currents will not equal zero.

The proposed protection scheme requires obtaining current phasor measurements from different locations throughout the network and comparing them during the same time frame. Differential protection is intended to be instantaneous. Thus, the electric network should be equipped with rapid standard-based communication capabilities. The proposed protection scheme will be ineffective on any electric grid without reliable and high-speed communication.

Numerous protection schemes based on communication are documented in the literature [5, 31, 33, 34]. Several of them require phasor quantities to function properly. Additionally, some commercially available digital relays have communication capabilities and time-synchronized

measurements [48]. Furthermore, smart current sensors can provide real-time measurements for grid monitoring, protection, and control [49, 50]. The proposed protection scheme is feasible and appropriate for microgrid protection due to the presence of these devices.

Chapter 3

Simulation

3.1 Introduction

As previously stated, the proposed differential zone protection scheme is a novel technique. It is critical to simulate this protection scheme in order to validate it and assess its influence on microgrids, particularly in the islanded mode of operation.

Two software packages are employed in this simulation. MATLAB Simulink [51] is the first software, while DIgSILENT PowerFactory [52] is the second. Simulink is used to create and simulate the protection scheme model for validation purposes. While DIgSILENT PowerFactory simulates the proposed protection scheme's impact on microgrids in two scenarios, one with and one without inverter-based resources.

In Simulink, the protection system is designed and validated without any switching actions. The protection system is tested by taking current measurements from the IEEE 13-node microgrid. The protective relays will act after comparing the current phasor measurements and sending a trip signal to the corresponding circuit breaker. On the other hand, DIgSILENT PowerFactory is a powerful software package for simulating power system dynamics. Thus, DIgSILENT simulates the proposed protection scheme's impact on the microgrid. In these simulations, the protection system is substituted by switching events that mimic the relays' operations.

Section 3.2 of this chapter illustrates the microgrid network that will be simulated. In Section 3.3, the proposed protection scheme is developed and validated by deploying it to the microgrid network. The impact of the protection scheme on the microgrid network is simulated in sections 3.4 and 3.5 considering two scenarios. Finally, in Section 3.6, a discussion of the simulation findings is presented.

3.2 Microgrid Application System

Microgrids are quite often connecting to a hosting distribution networks. The proposed protection scheme uses a small distribution network as a microgrid model. IEEE 13-node test feeder [53, 54], provides an excellent mechanism for simulating the proposed protection scheme. Although the size of the IEEE 13-node test feeder is modest, it exhibits some intriguing properties. This test feeder is compact and has a rather large load capacity. It is equipped with a single substation voltage regulator, which is composed of a three-phase unit coupled in Y. Besides that, it has overhead lines and underground cables phasing variety. Additionally, it has shunt capacitor banks and an in-line transformer. Furthermore, the loads on this test feeder are unbalanced and distributed. Reference[54] contains the complete data for the IEEE 13-node test feeder. The microgrid based on the IEEE 13-node test feeder is depicted in Figure 3.1.

By adding a generation sources and main connecting switch, this test feeder is viewed as a microgrid. The main connecting switch will be installed between bus 650 and bus 632, after the voltage regulator. This switch determines whether the microgrid operates in the grid-connected or isolated mode. This thesis is concerned with microgrids that operate in islanded mode; hence, all simulations will assume that the main connecting switch is open.

The microgrid is equipped with three synchronous generators in the first simulated scenario.

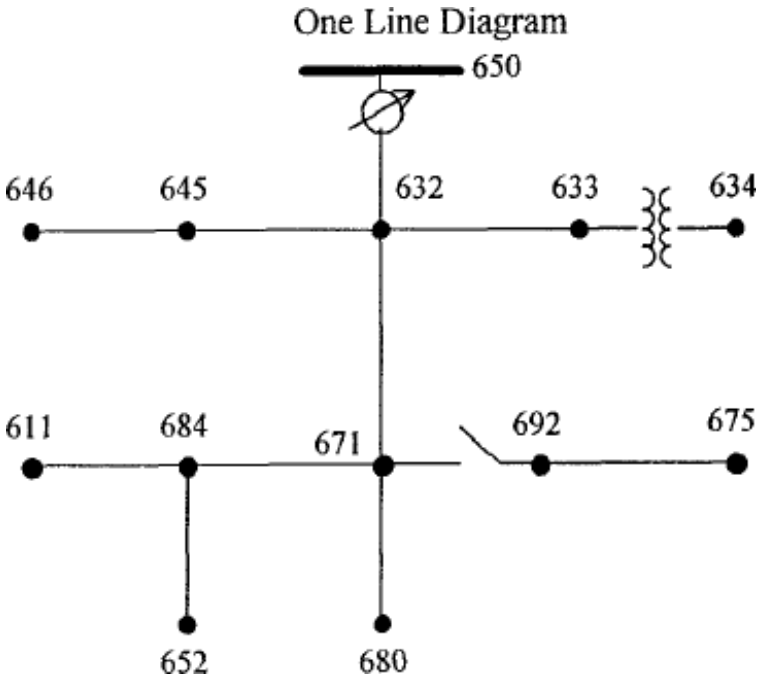

Figure 3.1: The IEEE 13-node test feeder

These generators, which are located at nodes 633, 675, and 680, have a total capacity of 1375 kVA, 2187.5 kVA, and 1375 kVA, respectively. These generators are equipped with the SEXS automatic voltage regulators (AVR) and a DEGOV1 governor speed control with a droop of 5%. The microgrid employed in the first scenario is depicted in Figure 3.2 as a single-line diagram.

In the second simulated scenario, the microgrid is equipped with two inverter-based resources (IBRs). These IBRs are a grid following photovoltaic (PV-GFLI) and a droop control grid-forming battery energy storage system (BESS-GFMI) with a droop of 1%. These IBRs are installed on bus 634 with a capacity of 500 kVA for the PV-GFLI and a capacity of 125 kVA for the BESS-GFMI. The microgrid employed in the second scenario is depicted in Figure 3.3 as a single-line diagram.

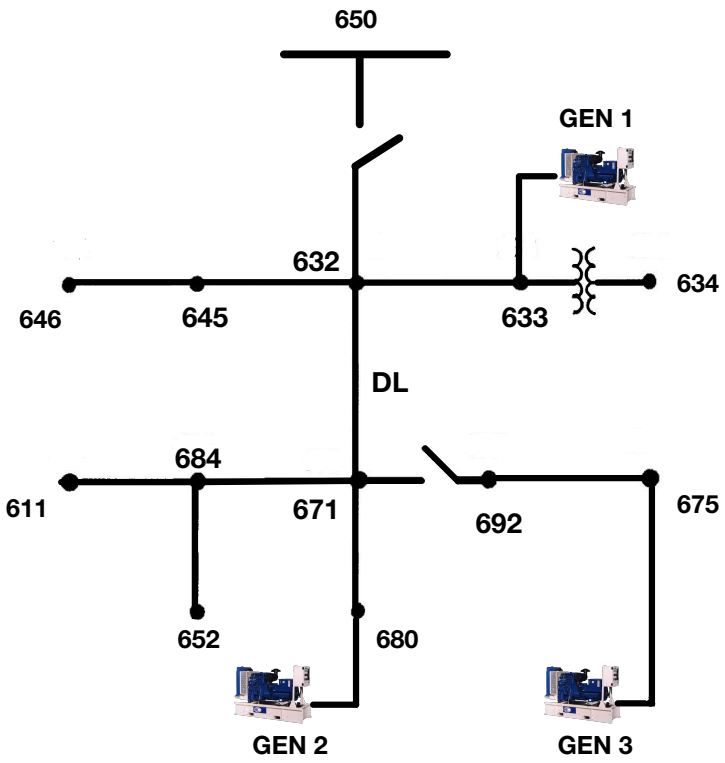

Figure 3.2: The Microgrid system without IBRs used in the first scenario.

3.3 Proposed Protection Scheme Design and Validation

3.3.1 Proposed Protection Scheme Design

Chapter 2 of this thesis discusses the proposed protection scheme in depth. The proposed protection scheme is applied and validated in this section on an IEEE 13-node microgrid. The first stage in implementing the proposed protection scheme is to calculate the power flow through the line. Then, depending on the power flow results, the graph partitioning algorithm could be applied to the microgrid. Table 3.1 summarizes the power flow results for the microgrid lines.

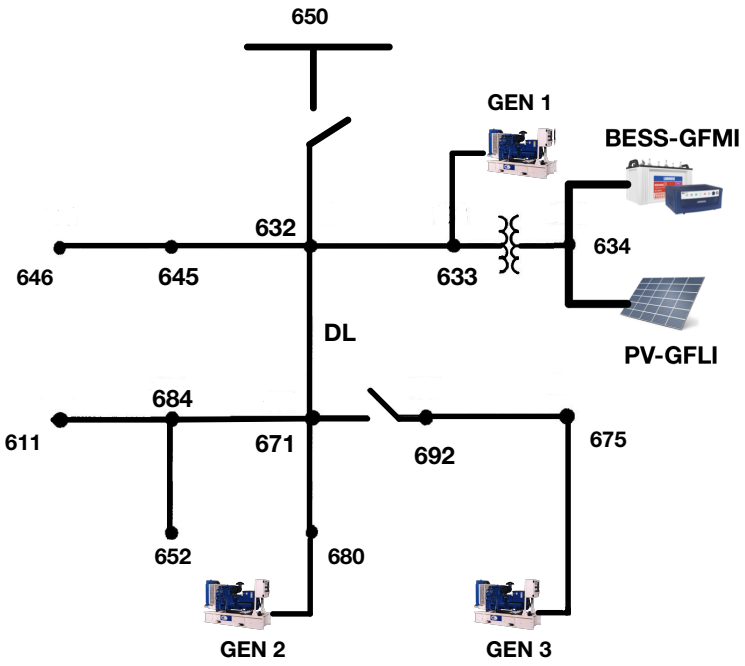

Figure 3.3: The Microgrid system with IBRs used in the second scenario.

Table 3.1: Microgrid line's power flow.

Line	Power flow in kW
Line 634-633	405.3
Line 633-632	592.9
Line 632-645	403.1
Line 645-646	230.5
Line 632-DL	189.7
Line DL-671	12.7
Line 671-692	0.31
Line 692-675	639.3
Line 671-680	998
Line 671-684	299.4
Line 684-652	128.7
Line 684-611	170.4

Five steps form the graph partitioning algorithm. The IEEE 13-node microgrid can be partitioned into small protection zones using these steps. The steps of the graph partitioning algorithm are as follows:

Step 1: Convert the IEEE 13-node microgrid to a graph with edge weights. The microgrid's graph network is seen in Figure 3.4.

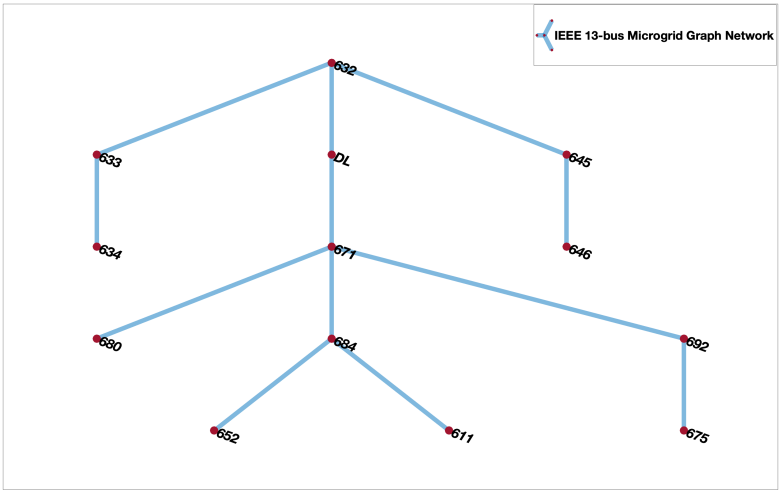

Figure 3.4: IEEE 13-node microgrid graph network.

Step 2: Calculate the Laplacian matrix Q, as well as its eigenvalues and eigenvectors.

Step 3: Create the partitioning matrix P using the first two eigenvectors of the Laplacian matrix Q.

Step 4: Select seeds for each of the two partitioned areas.

Step 5: Allocate the remaining vertices into the two partitioned areas.

This microgrid is divided into two protection zones using the graph partitioning algorithm. The microgrid cannot be further divided into more than two zones due to the microgrid's

impracticality. The first protection zone is composed of the nodes 634, 633, 632, 645, and 646, as well as the distributed load DL. The first zone is comprised of a single synchronous generator with a capacity of 1375 kVA, a total load capacity of 1000 kW, and 663 kVar. The second protection zone, on the other hand, comprises nodes 675, 692, 671, 680, 684, 652, and 611. Additionally, the second zone contains two synchronous generators with a combined capacity of 3562.5 kVA, a load capacity of 2466 kW, and 739 kVar.

Four digital relays are required to implement the proposed protection scheme. Each generator bus will have a digital relay installed to measure the current entering the zones, and bus 671 will have one relay installed between zones 1 and 2. On the other hand, the number of smart current sensors required is equal to the number of microgrid loads. Thus, nine smart current sensors are required, assuming that only one sensor is required for distributed loads. To implement the proposed protection scheme for the IEEE 13-node microgrid, four digital relays and nine smart current sensors are required. The proposed protection scheme for the IEEE 13-node microgrid is summarized in Table 3.2.

Table 3.2: Summary of the proposed protection scheme for the IEEE 13-node microgrid.

	Zone 1	**Zone 2**
Nodes	634, 633, 632, 645, 646, DL	675, 692, 671, 680 ,684, 652, 611
Generation sources	1	2
Installed capacity	1375 kVA	3562.5 kVA
Load consumption	1000 kW	2466 kW
Digital relays	4	
Smart current sensors	9	

3.3.2 Proposed Protection Scheme Validation

After completing the design of the proposed protection scheme, it is important to validate it. The differential zone protection scheme should be capable of detecting faults and isolating just the faulty zone. To validate the protection system, two simulated scenarios are required. At t=100s, a three-phase to ground fault occurs in zone 1 between nodes 633 and 632 in the first scenario. This scenario evaluates the protection system's response to faults originating in zone 1. Zone 1's differential zone protection should identify the fault and adequately isolate it. On the other hand, zone 2's differential zone protection should remain unaffected by the fault and should not isolate zone 2. The second simulation scenario is identical to the first, besides the location of the fault in zone 2, between nodes 675 and 692. The first simulation scenario is depicted in Figures (3.5,3.6,3.7, and 3.8), whereas the second simulation scenario is depicted in Figures (3.11,3.12,3.9, and 3.10).

The total current entering zone 1 is depicted in Figure 3.5a, and the total current exiting zone 1 is depicted in Figure 3.5b. As seen in Figure 3.5, the currents from sources grow substantially during the fault and reach a maximum value of around 11 kA, whereas total current exiting zone 1 decreased by around 90% of its typical value.

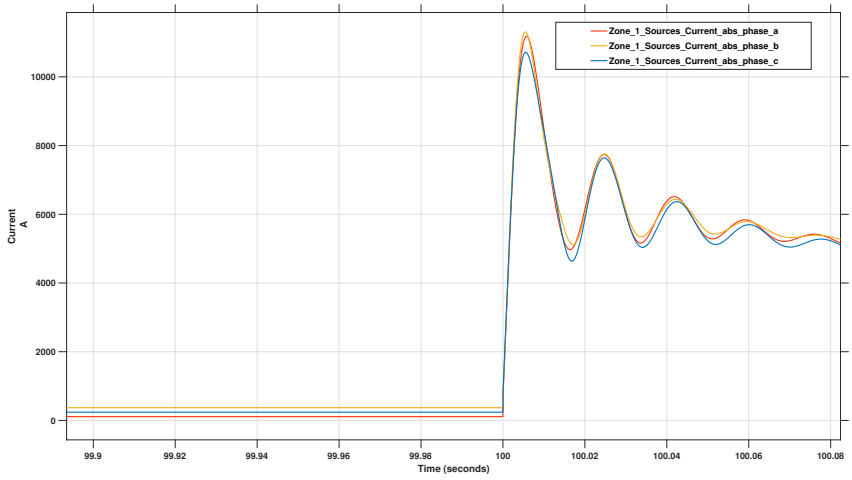

(a) Sources Currents.

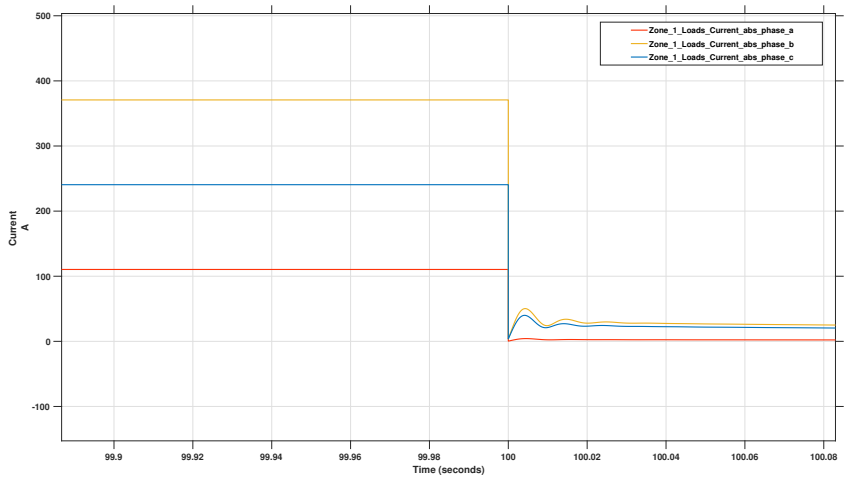

(b) Loads Currents

Figure 3.5: Zone 1 sources and loads current magnitudes during fault occurs in zone 1.

The magnitude of the differential current in zone 1 is depicted in Figure 3.6a. After a fault occurs, the differential current increases substantially and returns to zero after 83.3 milliseconds when the fault is cleared. The tripping signal for zone 1 relays is depicted in Figure 3.6b. When a fault occurs in zone 1, the relays detect it and send a trip signal to the corresponding circuit breakers.

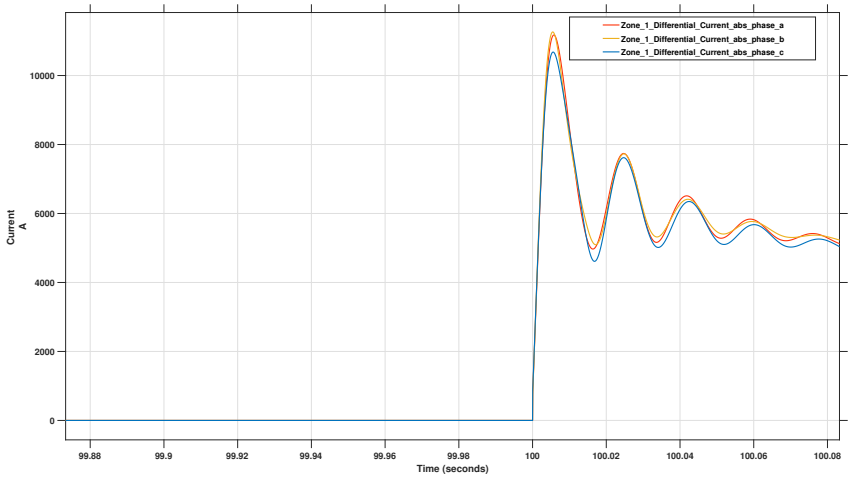

(a) Differential current magnitude.

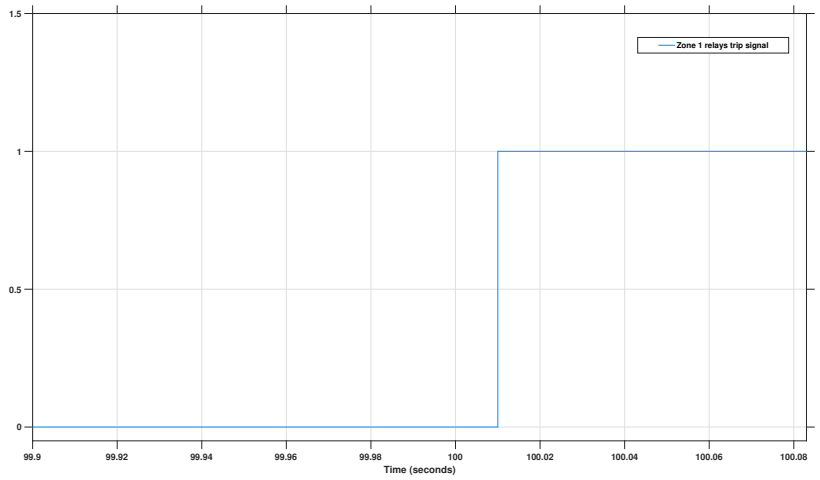

(b) Relay trip signal.

Figure 3.6: Zone 1 Differential current magnitude and relay trip signal during fault occurs in zone 1.

Figure 3.7a shows the total sources currents of zone 2, whereas figure 3.7b shows the total loads current within zone 2. During the fault, the currents of the sources and loads fell by up to 70% of their normal values. However, the differential current remains approximately zero, as seen in figure 3.8a. Thus, the relays at zone 2 did not send a trip signal to the corresponding circuit breakers, as seen in figure 3.8a.

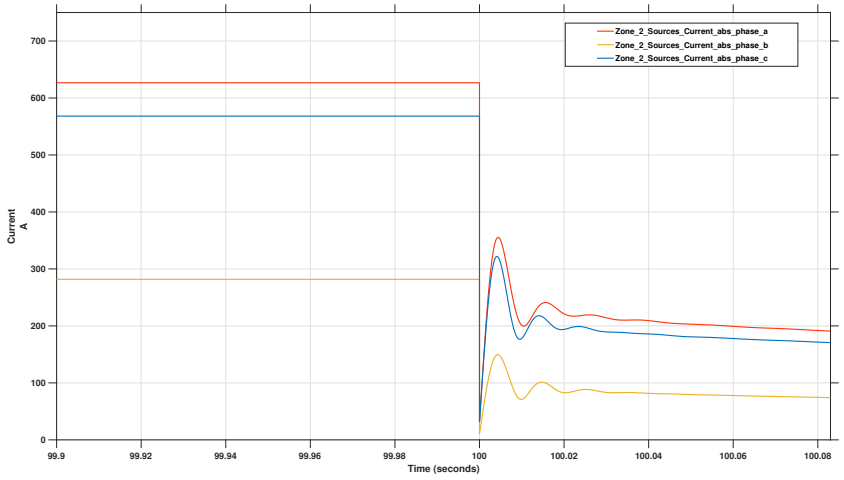

(a) Sources Currents.

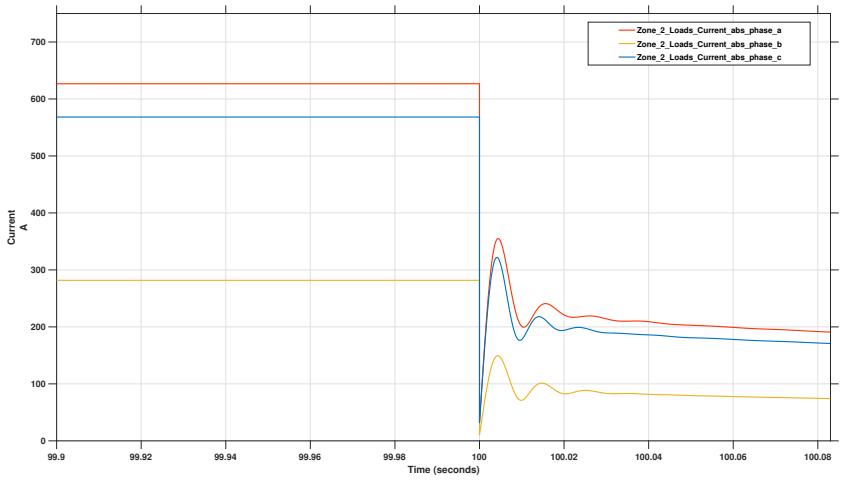

(b) Loads Currents

Figure 3.7: Zone 2 sources and loads current magnitudes during fault occurs in zone 1.

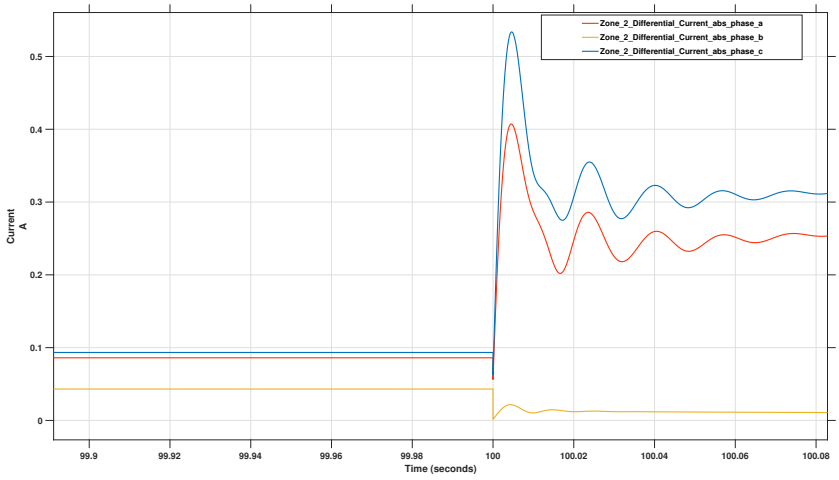

(a) Differential current magnitude.

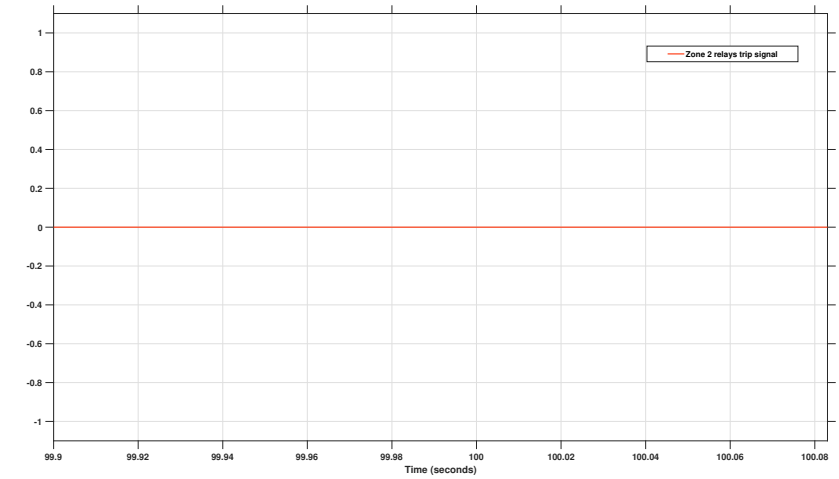

(b) Relay trip signal.

Figure 3.8: Zone 2 Differential current magnitude and relay trip signal during fault occurrence in zone 1.

In the second simulated scenario, a fault occurs between nodes 675 and 692. The total sources currents in zone 1 are shown in Figure 3.9a, while the total loads' currents in zone 1 are shown in Figure 3.9b. Currents from both sources and loads decreased by up to 80% of their normal values during the fault. However, as seen in Figure 3.10a, the differential current stays roughly zero. Thus, as seen in Figure 3.10b, the relays in zone 2 did not send

a trip signal to the corresponding circuit breakers.

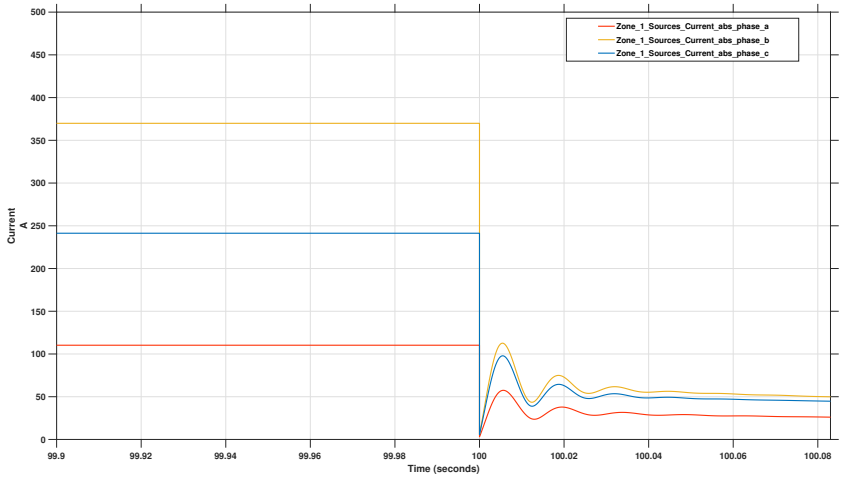

(a) Sources Currents.

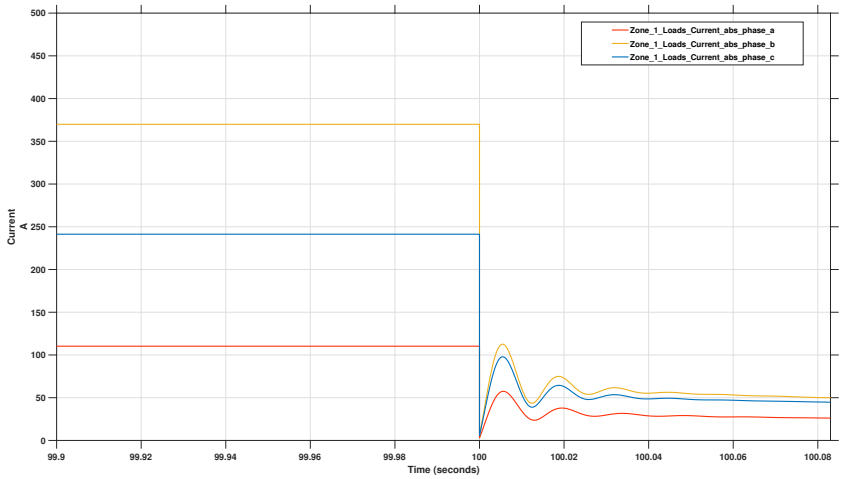

(b) Loads Currents

Figure 3.9: Zone 1 sources and loads current magnitudes during fault occurs in zone 2.

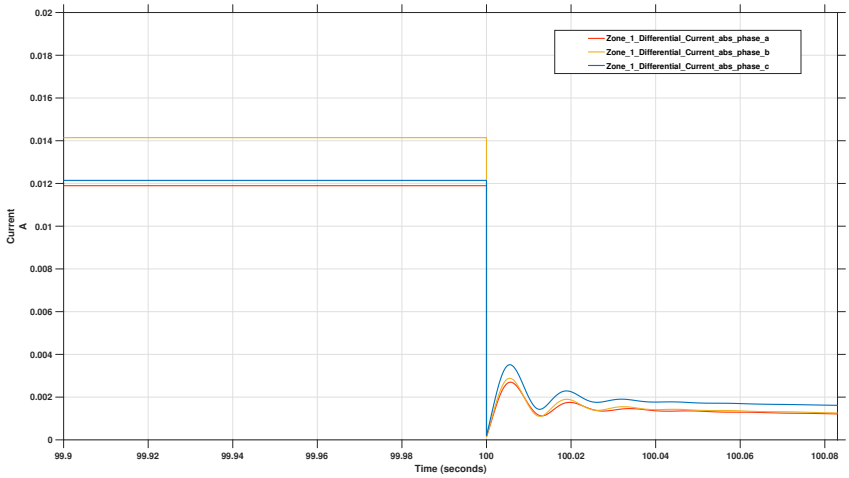

(a) Differential current magnitude.

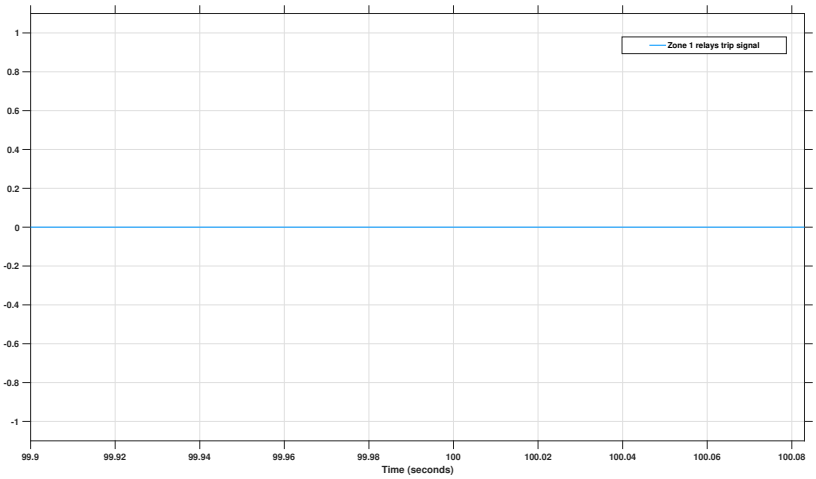

(b) Relay trip signal.

Figure 3.10: Zone 1 Differential current magnitude and relay trip signal during fault occurs in zone 2.

The total current entering zone 2 is illustrated in Figure 3.11a, and the total current exiting zone 2 is depicted in Figure 3.11b . As seen in Figure 3.11, currents from sources increase significantly throughout the fault and peak at roughly 14 kA, whereas the currents of zone 2 total load decreased by nearly 95% of their normal values.

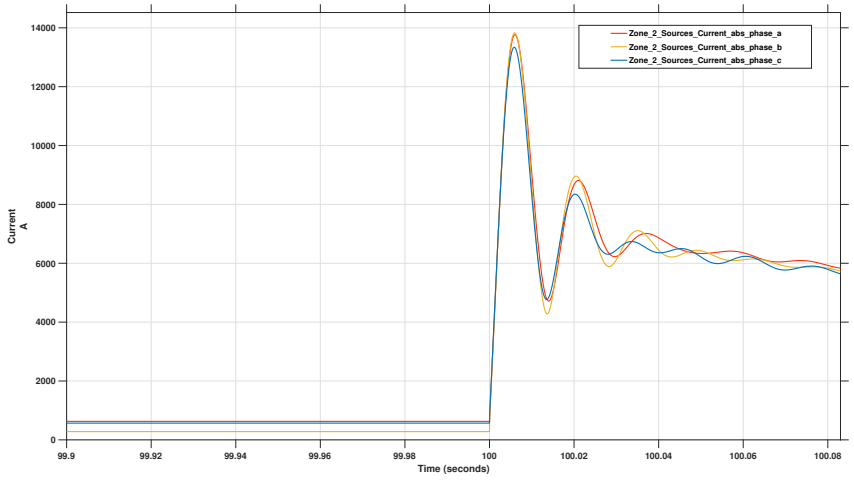

(a) Sources Currents.

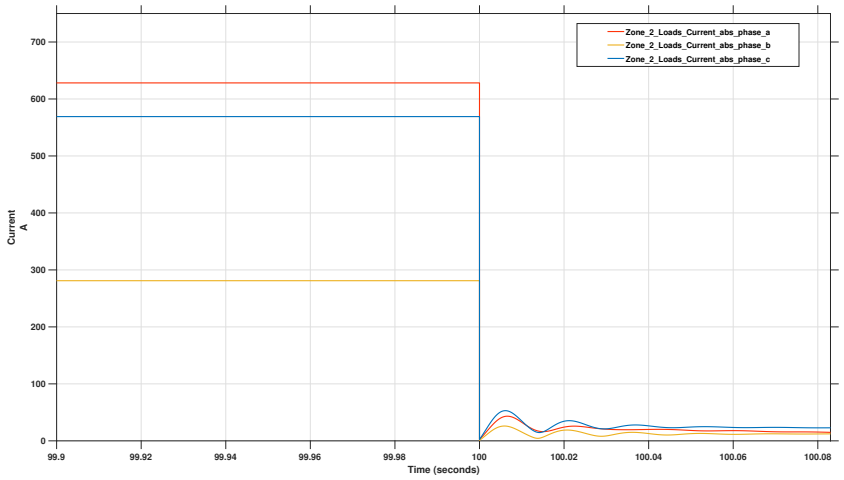

(b) Loads Currents

Figure 3.11: Zone 2 sources and loads current magnitudes during fault occurs in zone 2.

Figure 3.12a shows the magnitude of the differential current in zone 2. When a fault occurs, the differential current grows significantly and then returns to zero after 83.3 milliseconds. Figure 3.12b illustrates the tripping signal for zone 2 relays. When a fault occurs in zone 2, the relays detect it and send a trip signal to the corresponding circuit breakers.

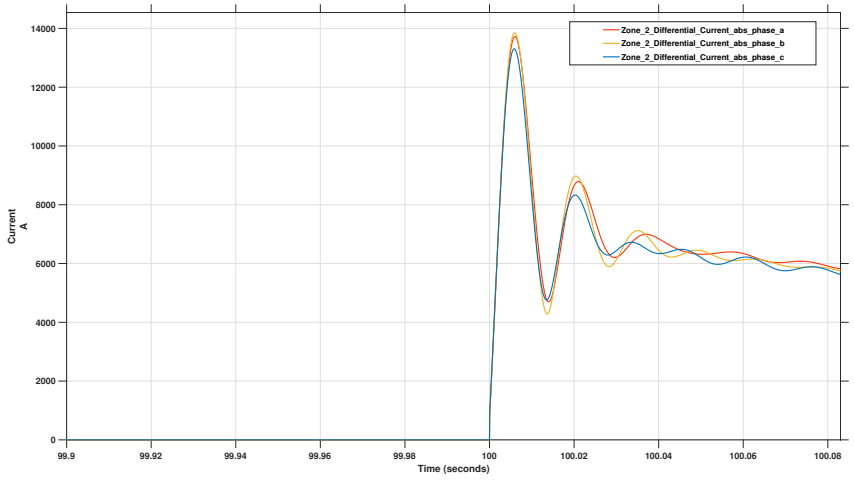

(a) Differential current magnitude.

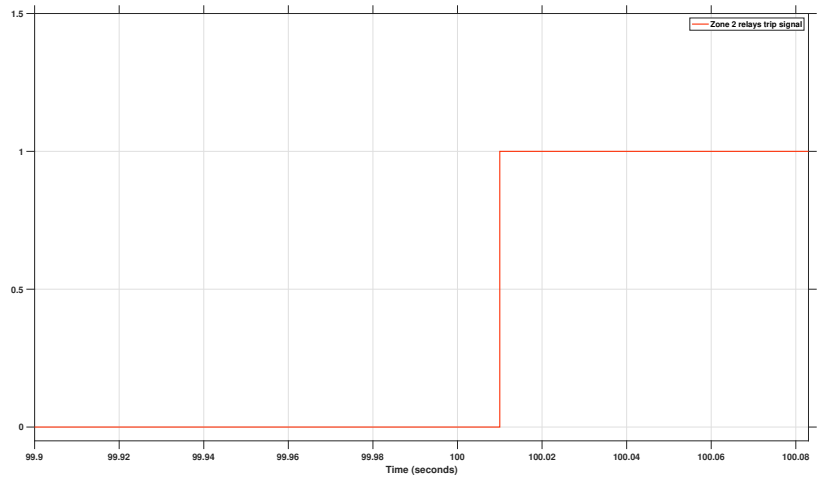

(b) Relay trip signal.

Figure 3.12: Zone 2 Differential current magnitude and relay trip signal during fault occurs in zone 2.

The proposed protection scheme demonstrated that each protection zone has a sufficient generation and load balance when applied to the IEEE 13-node microgrid. Additionally, in the event of a fault, the protection system is capable of recognizing and isolating just the affected zones. The relays linked with zone 1 detected the fault inside zone 1, but ignored the fault in zone 2. Zone 2 relays, on the other hand, detect faults inside zone 2 and ignore

faults in zone 1.

3.4 Case 1: Impact on Microgrid without Inverter-Based Resources

The proposed protection scheme's influence on the microgrid is simulated in this section using the DIgSILENT PowerFactory software [52]. Three distributed generators with capacities of 1375 kVA, 2187.5 kVA, and 1375 kVA will be installed at nodes 633, 675, and 680. These generators are equipped with the SEXS automatic voltage regulators (AVR) and a DEGOV1 governor speed control with a droop of 5%. In this case study, two simulation scenarios are conducted. The first simulation scenario utilizes a three-phase to a ground fault that occurs within zone 1, whereas the second simulation scenario utilizes a zone 2 three-phase to ground fault. The simulation will last 200 seconds in total, with the fault occurring at time t=100s and then being cleared after five cycles.

3.4.1 Fault Within Zone 1

Between nodes 633 and 632, a three-phase to ground fault occurs. The IEEE 13-node microgrid single-line diagram is shown in Figure 3.13. As seen in the Figure, the fault occurs in zone 1, and zone 1 is then isolated by the circuit breakers located at the generator 1 and node 671 busbars, while generators 2 and 3 continue to supply zone 2.

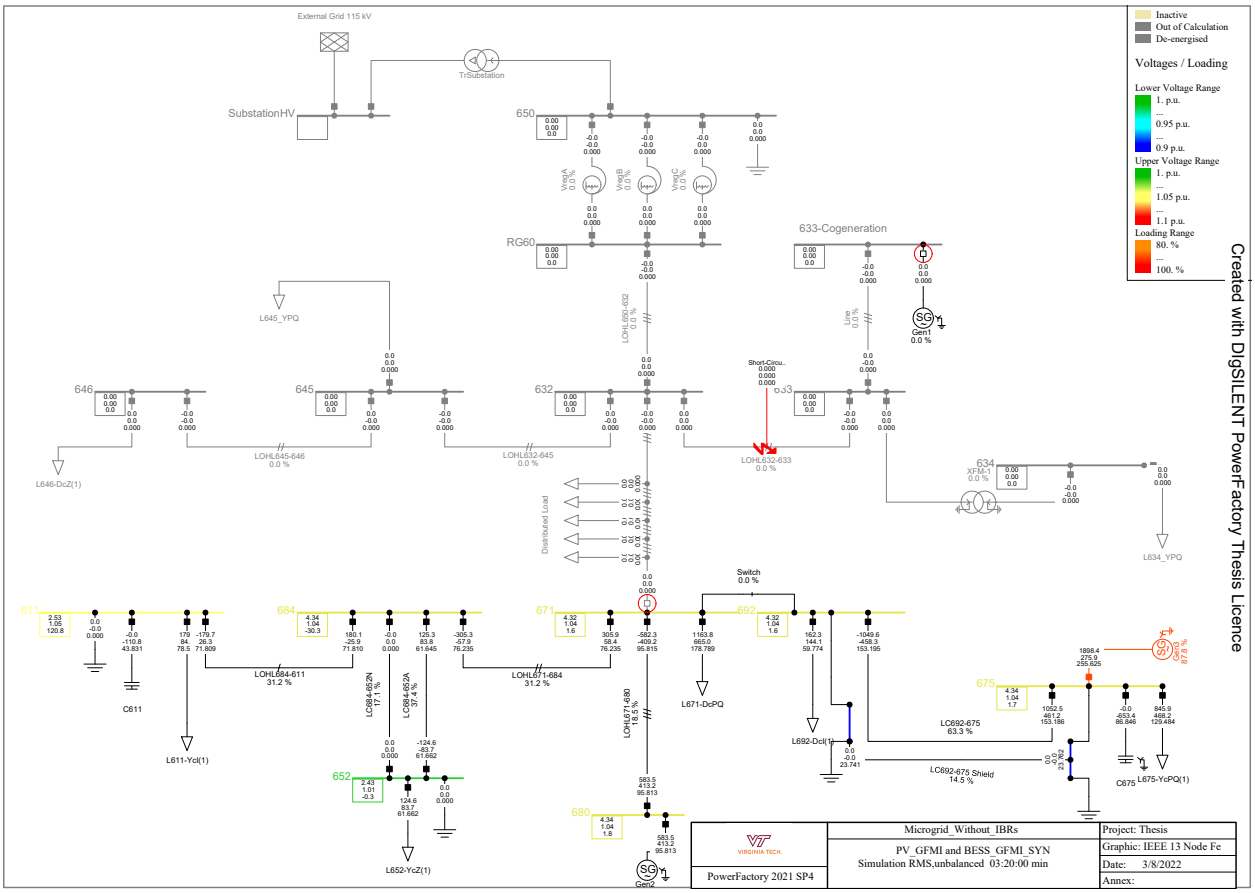

Figure 3.13: IEEE 13-node microgrid without IBRs during fault in zone 1.

The simulation of distributed generators in zone 2 is depicted in Figure 3.14. The active power of the generators is depicted in Figure 3.14a, while the reactive power of the generators is depicted in Figure 3.14b. As seen in the figures, once the fault was resolved, generators 2 and 3 active power dropped a little because zone 2 was supplying 300 kW to zone 1. The voltages of the generators are shown in Figure 3.14c, and the frequencies of the generators are shown in Figure 3.14d. After the fault is cleared, zone 2 generators frequency stabilizes at around 60.06 Hz. On the other hand, the voltage returns to normal after the fault is cleared.

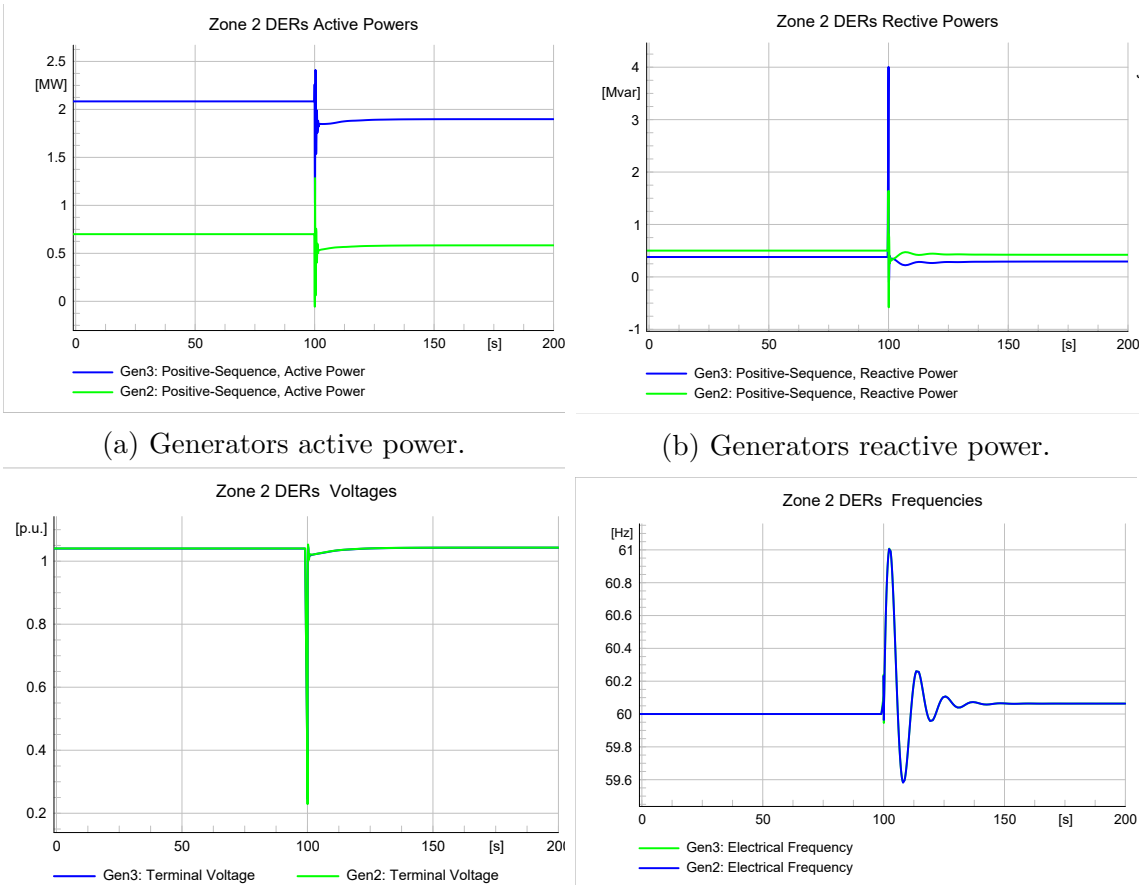

(a) Generators active power.

(b) Generators reactive power.

(c) Generators terminal voltages.

(d) Generators electrical frequencies.

Figure 3.14: Distributed generators simulation with fault in zone 1.

Zone 2 nodes voltages and frequencies are depicted in Figure 3.15. Figure 3.15a depicts zone 2 node voltages, whereas zone 2 node frequencies are depicted in Figure 3.15. As seen in the figures, once the fault is cleared, the voltages of zone 2 nodes return to normal values with slight changes in some node voltages. The frequencies of zone 2 node are almost identical to the generators frequency responses. the microgrid frequency fluctuated from 61 Hz to 59.6 Hz during transients until the system reaches steady state values within 20s.

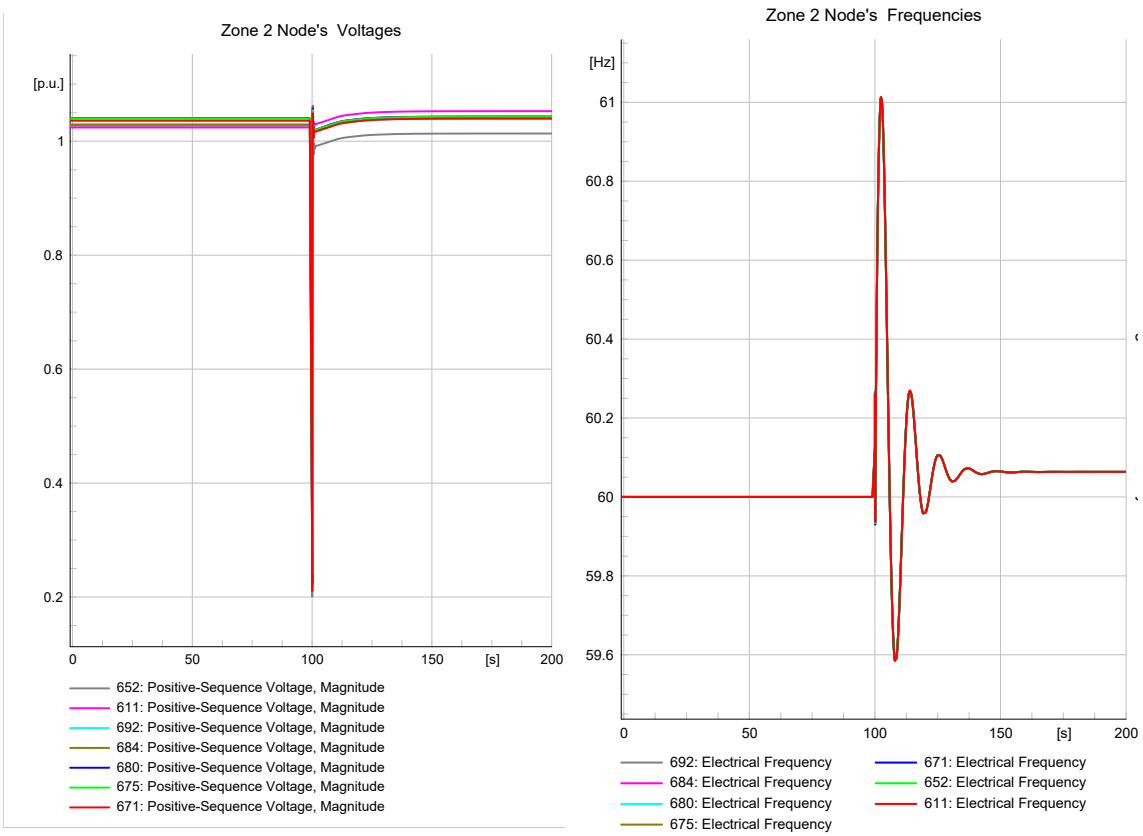

(a) Zone 2 nodes' voltages.

(b) Zone 2 nodes' frequencies.

Figure 3.15: Zone 2 nodes voltages and frequencies.

3.4.2 Fault Within Zone 2

An this scenario a three-phase to ground fault occurs in zone 2 between nodes 671 and 780. Figure 3.16 depicts the IEEE 13-node microgrid single-line diagram. Zone 2 is separated through circuit breakers positioned at generator 2 busbar, generator 3 busbar, and node 671 busbar. Generator 1, on the other hand, continues to feed zone 1.

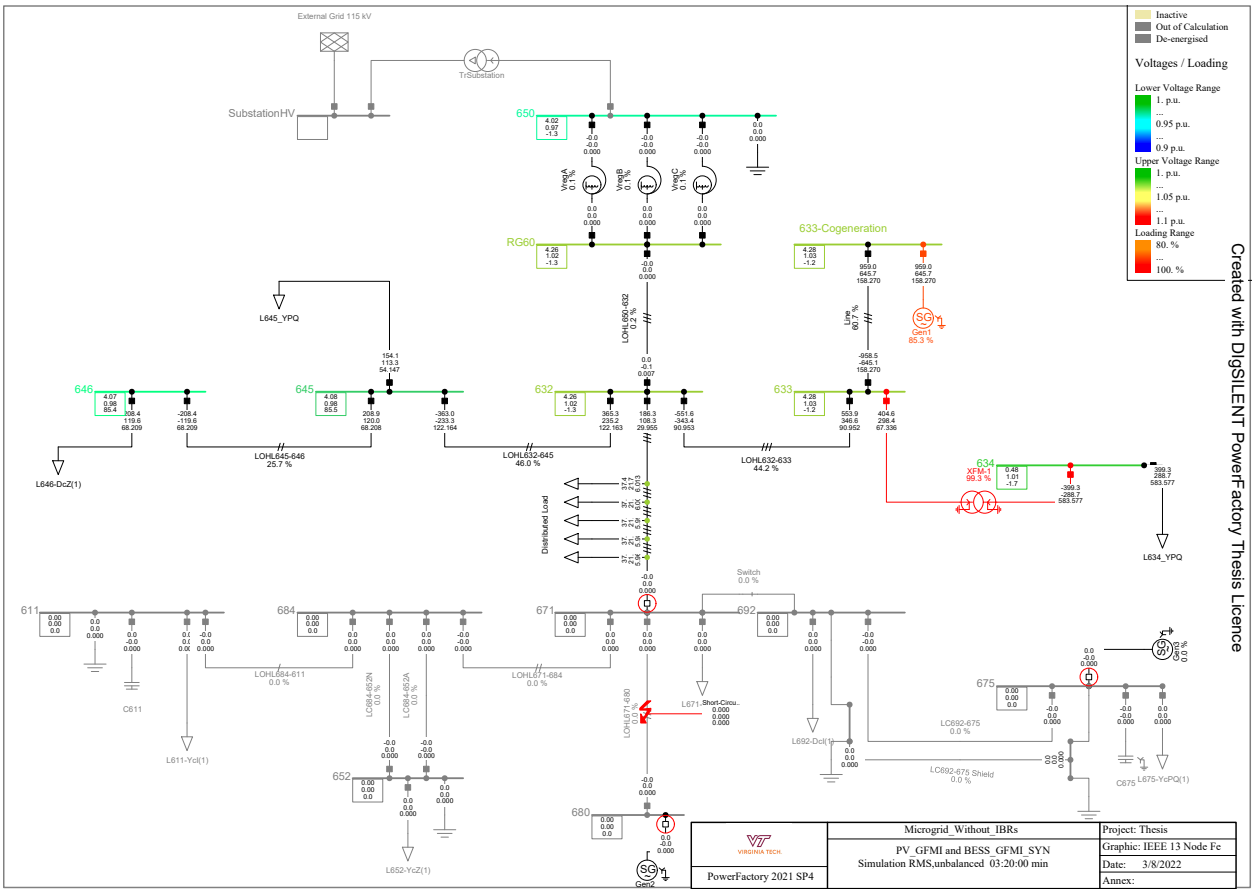

Figure 3.16: IEEE 13-node microgrid without IBRs during fault in zone 2.

The active power of zone 1 generator is depicted in Figure 3.17a, while the reactive power of the generator is depicted in Figure 3.17b. As seen in the figures, once the fault is resolved, generator 1 active power increases by around 260 kW and supplied the remaining zone. The voltages of the generator are shown in Figure 3.17c, and the frequencies of the generators are shown in Figure 3.17d. After the fault is cleared, generator 1 frequency fluctuates from 61 Hz to 58.5 Hz during transients then stabilizes at around 59.25 Hz within 20s. On the other hand, the generator voltage returns to normal with almost negligible decrease.

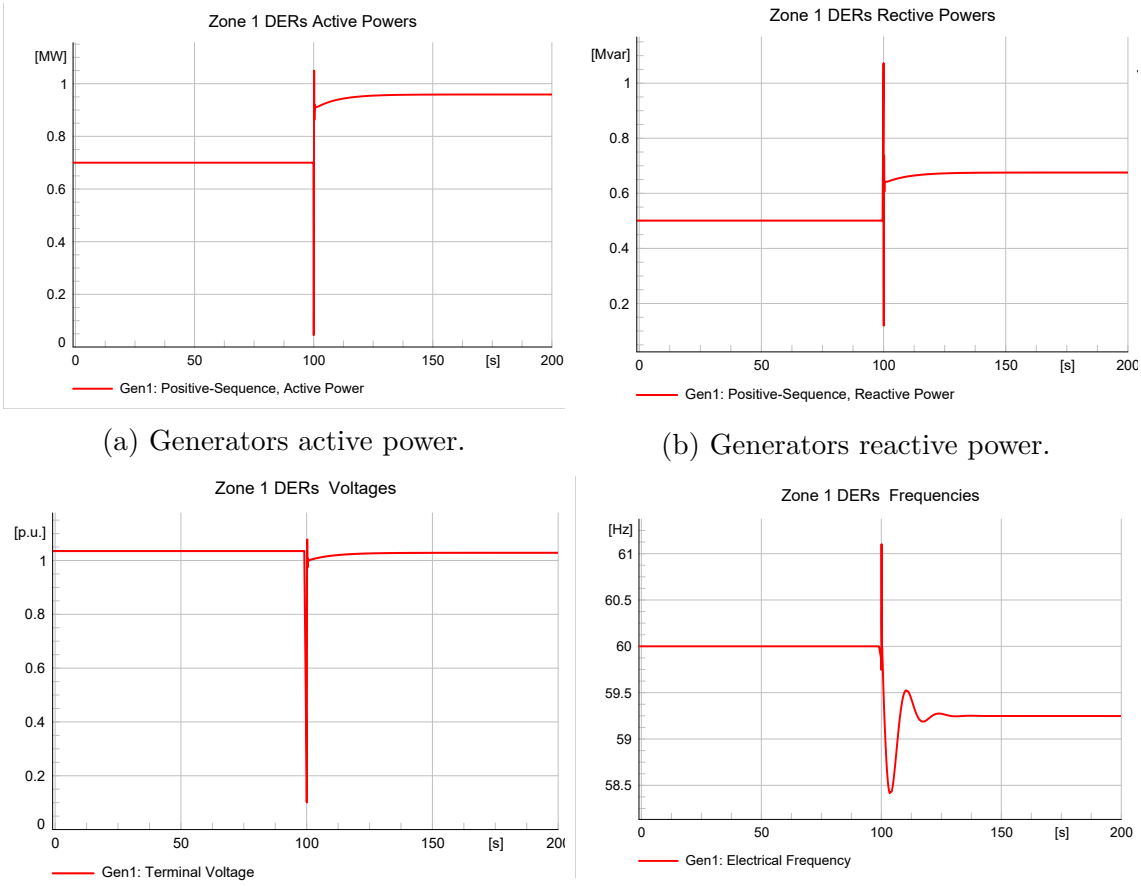

(a) Generators active power.

(b) Generators reactive power.

(c) Generators terminal voltages.

(d) Generators electrical frequencies.

Figure 3.17: Distributed generators simulation with fault in zone 2.

Finally, Figure 3.18a depicts the zone 1 node voltages and frequencies. Zone 1 node voltages are depicted in Figure 3.18a, whereas the frequencies are depicted in Figure 3.18b. After the fault is cleared, the voltages of zone 1 nodes return to normal values with slight changes in some node voltages. The frequencies of zone 1 nodes are almost identical to the generator frequency responses. the microgrid frequency fluctuates from 61 Hz to 58.5 Hz during transients until the system reaches steady state values within 20s.

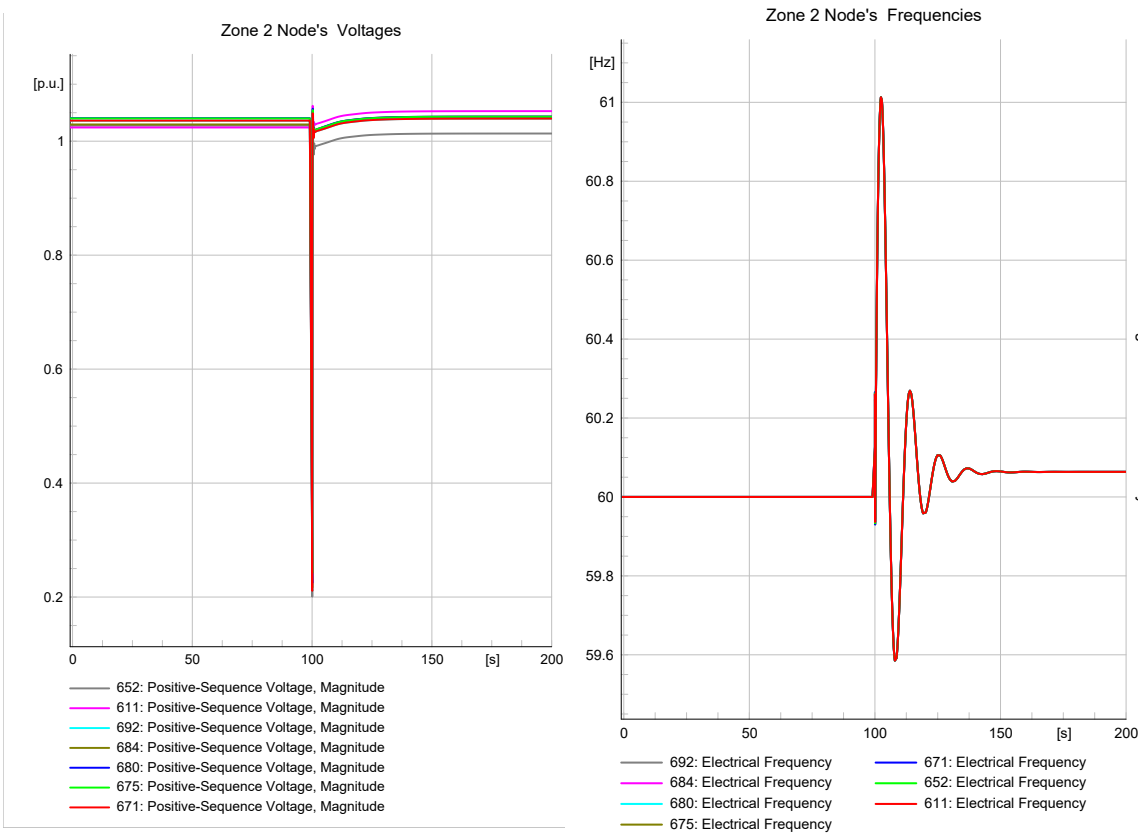

(a) Zone 1 nodes' voltages.

(b) Zone 1 nodes' frequencies.

Figure 3.18: Zone 1 nodes voltages and frequencies.

3.5 Case 2: Impact on Microgrid with Inverter-Based Resources

Five distributed energy resources (DERs) are installed in the IEEE 13-node microgrid. Three distributed generators with capacities of 1375 kVA, 2187.5 kVA, and 1375 kVA will be deployed at nodes 633, 675, and 680 in this case study. Additionally, the microgrid will be equipped with two IBRs. The first IBR is a 125 kW battery energy storage system with droop control grid-forming inverter (BESS-GFMI) that will be deployed at node 634.

The second IBRs is a 500 kW photovoltaic system with grid-following inverter (PV-GFLI) that will be installed in node 634. As in the previous section, two simulation scenarios are conducted with a fault in zone 1 and another with a fault in zone 2. The simulation will last 200 seconds in total, with the fault occurring at time t=100s and then being cleared after five cycles.

3.5.1 Fault Within Zone 1

A three-phase to ground fault occurs between nodes 633 and 632. The IEEE 13-node microgrid single-line diagram is shown in Figure 3.19. As seen in the figure, the fault occurs in zone 1, and zone 1 is then isolated by the circuit breakers located at the generator 1, BESS, PV, and node 671 busbars. While generators 2 and 3 continue to supply zone 2.

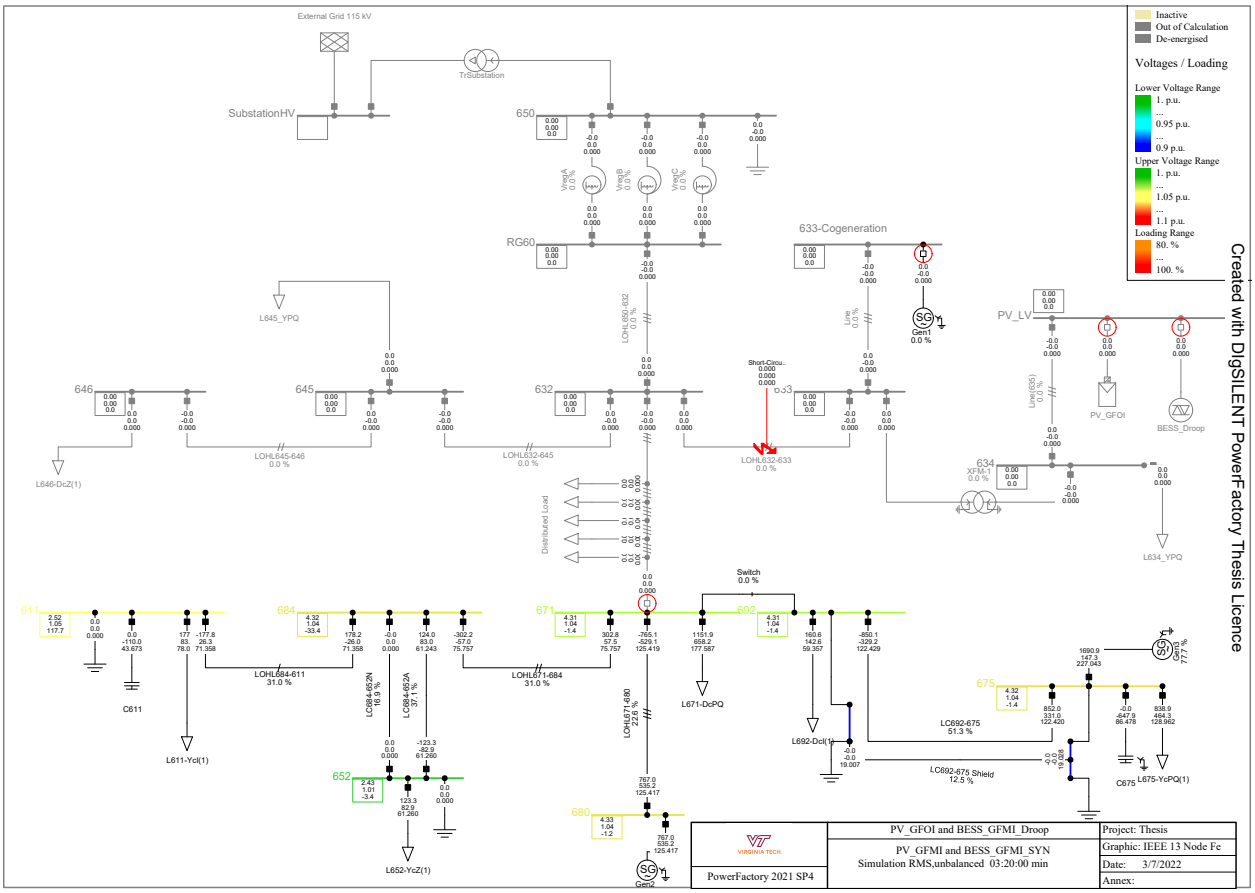

Figure 3.19: IEEE 13-node microgrid with IBRs during fault in zone 1.

The simulation of distributed generators in zone 2 is depicted in Figure 3.20. The active power of the generators is depicted in Figure 3.20a, while the reactive power of the generators is depicted in Figure 3.20b. As seen in the figures, once the fault is resolved, generators 2 and 3 active power increases a little because zone 1 is supplying 170 kW to zone 2. The voltages of the generators are shown in Figure 3.20c, and the frequencies of the generators are shown in Figure 3.20d. After the fault is cleared, zone 2 generator frequency stabilizes at around 59.96 Hz. On the other hand, the voltage returns to normal after the fault is cleared.

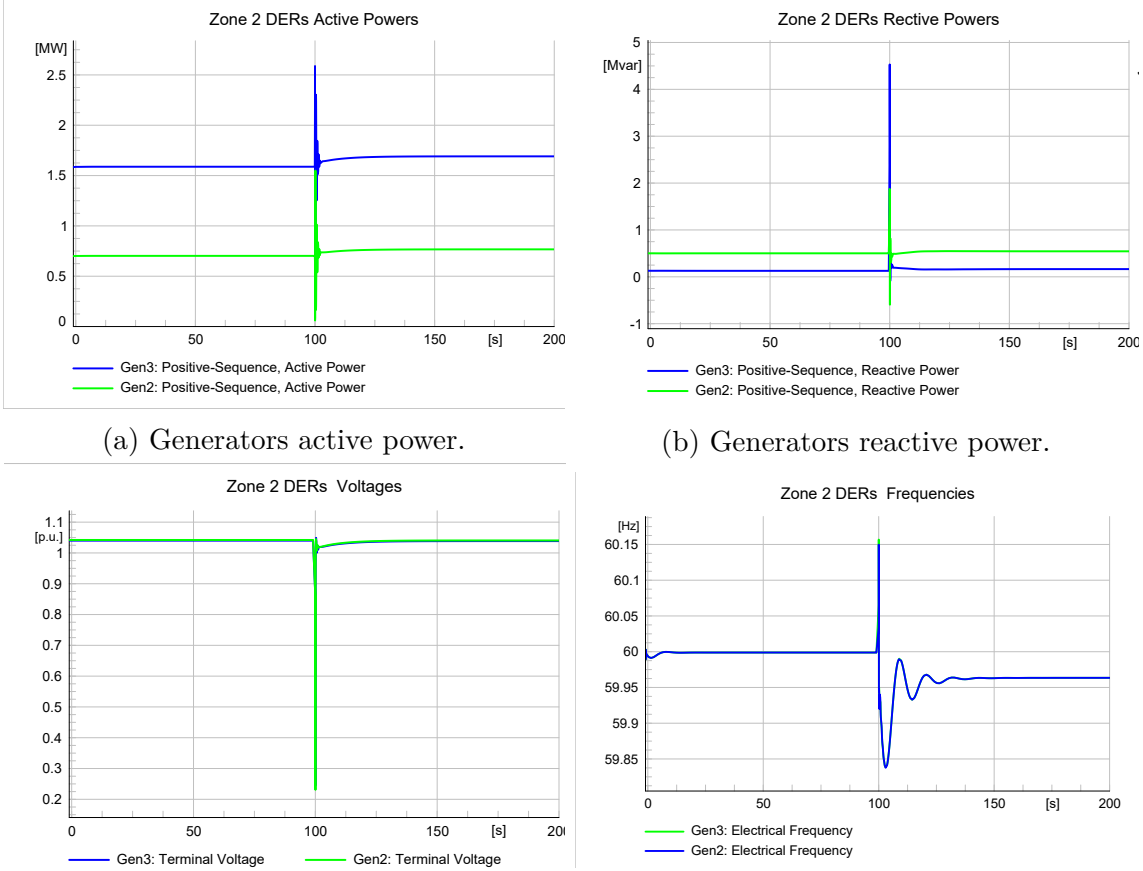

(a) Generators active power.

(b) Generators reactive power.

(c) Generators terminal voltages.

(d) Generators electrical frequencies.

Figure 3.20: Distributed generators simulation with fault in zone 1.

Zone 2 nodes voltages and frequencies are depicted in Figure 3.21. Figure 3.21a depicts zone 2 node voltages, whereas zone 2 node frequencies are depicted in Figure 3.21. As seen in the figures, once the fault is cleared, the voltages of zone 2 nodes return to normal values with slight changes in some node voltages. The frequencies of zone 2 nodes are almost identical to the generator frequency responses. The microgrid frequency fluctuates from 60.15 Hz to 59.8 Hz during transients until the system reaches steady state values within 20s.

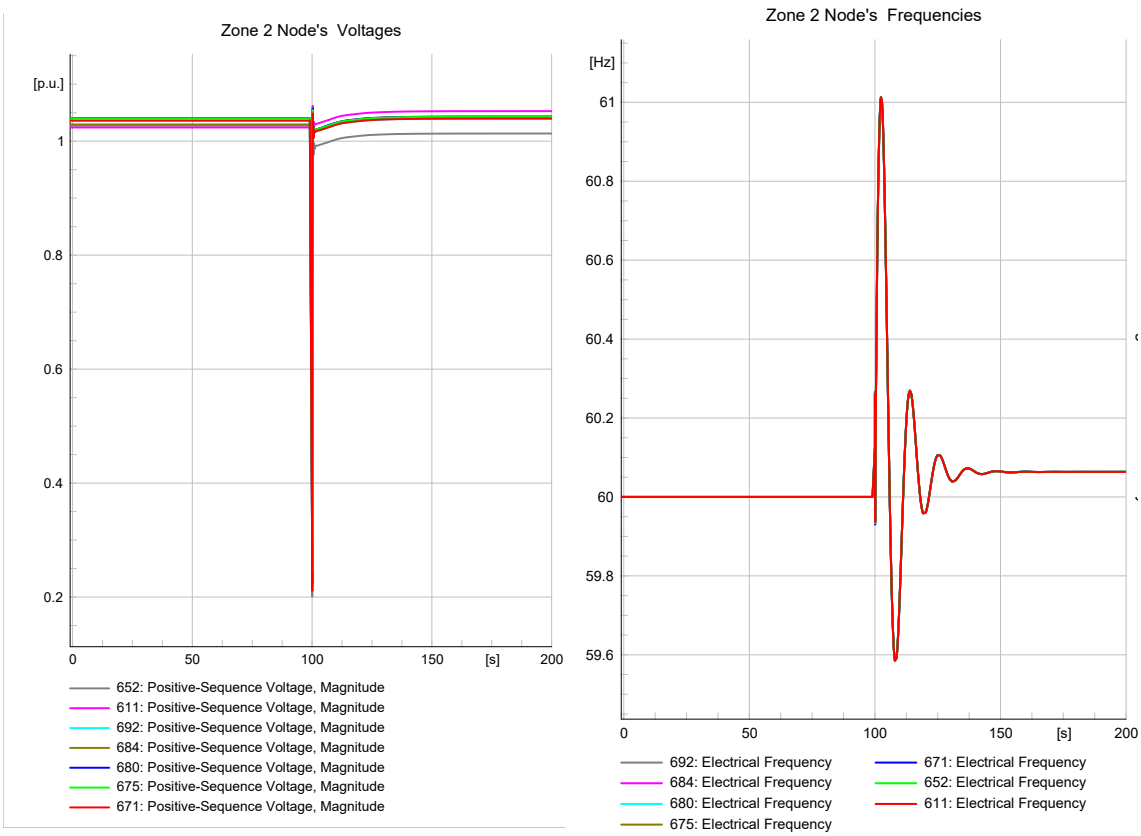

(a) Zone 2 nodes' voltages.

(b) Zone 2 nodes' frequencies.

Figure 3.21: Zone 2 nodes voltages and frequencies.

3.5.2 Fault Within Zone 2

In this scenario, a three-phase to ground fault occurs in zone 2 between nodes 671 and 680. The IEEE 13-node microgrid single-line diagram is shown in Figure 3.22. Zone 2 is divided by circuit breakers located at the generator 2,generator 3 and node 671 busbars. On the other hand, generator 1, BESS, and PV continue to supply zone 1.

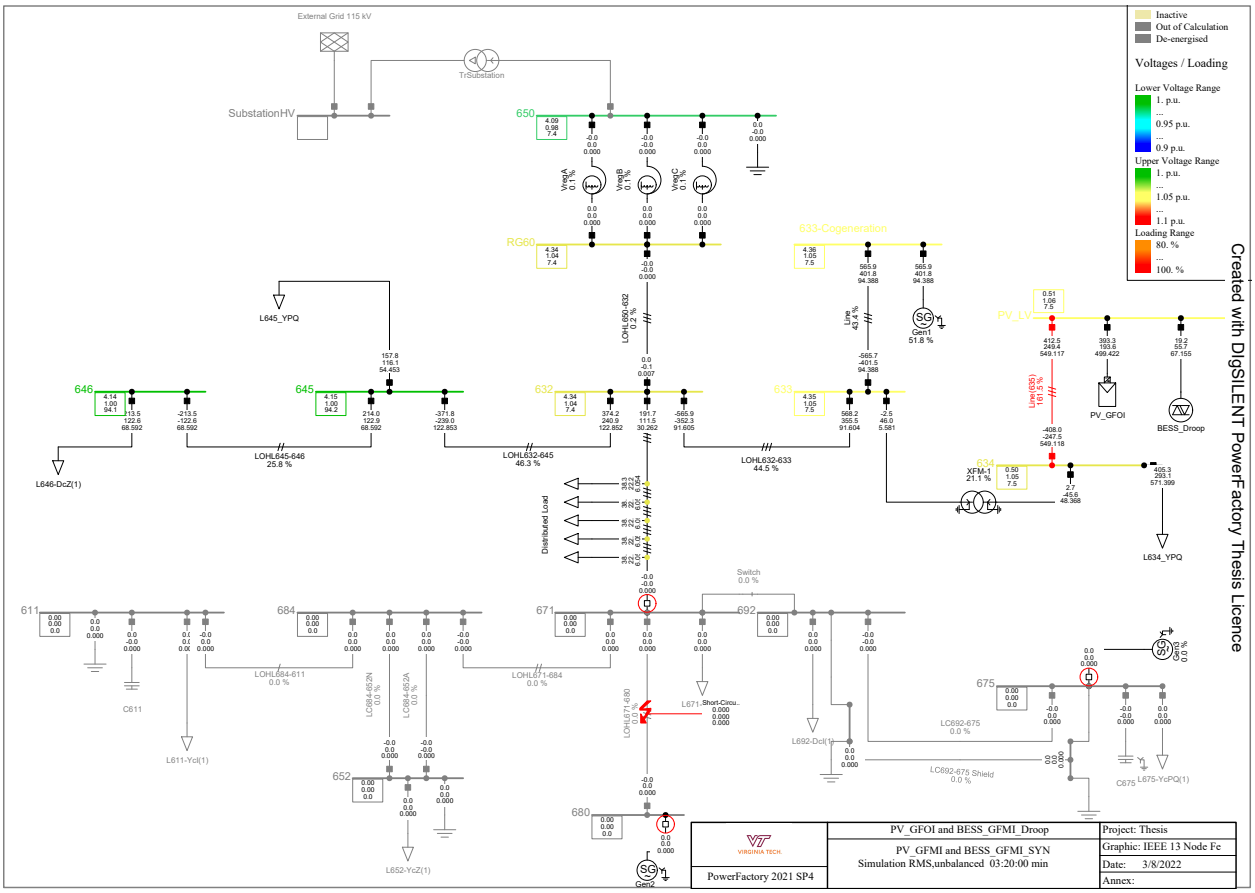

Figure 3.22: IEEE 13-node microgrid with IBRs during fault in zone 2.

The active power of zone 1 generator is depicted in Figure 3.23a, while the reactive power of the generator is depicted in Figure 3.23b. As seen in the figures, once the fault is resolved, zone 1 DERs active power decreases by around 170 kW and supplied the remaining zone. The voltages of the DERs are shown in Figure 3.23c, and the frequencies of the DERs are shown in Figure 3.23d. After the fault is cleared, zone 1 DERs frequencies fluctuate from 61.4 Hz to 57.6 Hz during transients then stabilize at around 60.39 Hz within 15 s. On the other hand, the generator voltage returns to normal with almost negligible decrease.

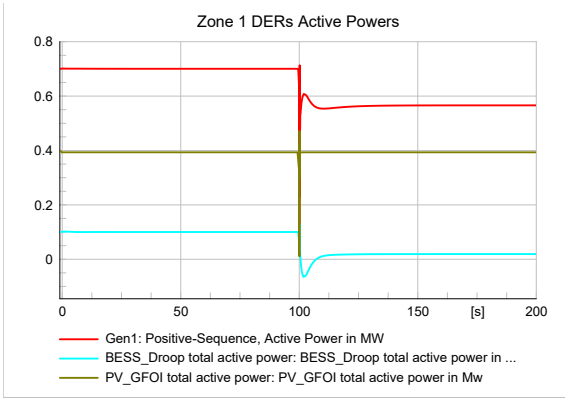

(a) Generators active power.

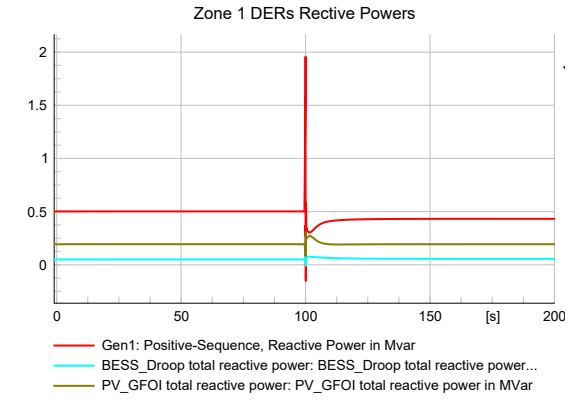

(b) Generators reactive power.

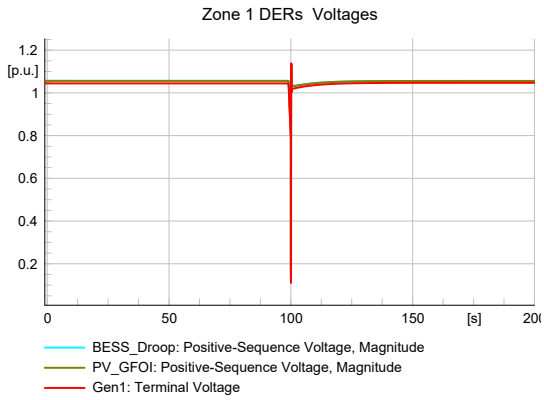

(c) Generators terminal voltages.

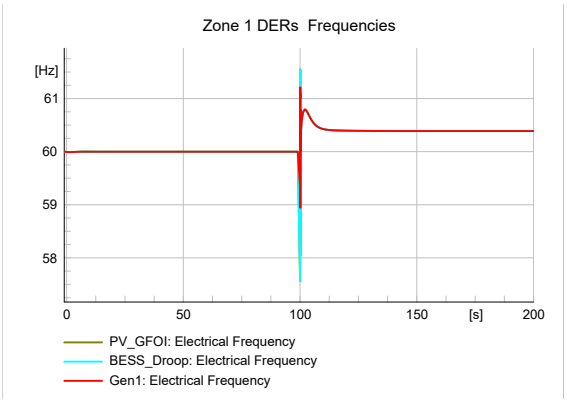

(d) Generators electrical frequencies.

Figure 3.23: Distributed generators simulation with fault in zone 2.

Generator 1 power supplies drop from 700 kW to 565 kW and the BESS power supplies drop from 100 kW to 19 kW, while the PV power supplies stay at 400 kW. Both Generator 1 and the BESS has a droop control, thus their supplies dropped based on their droop percentage. Figure 3.24 shows the frequency droop characteristics for both generator 1 and the BESS.

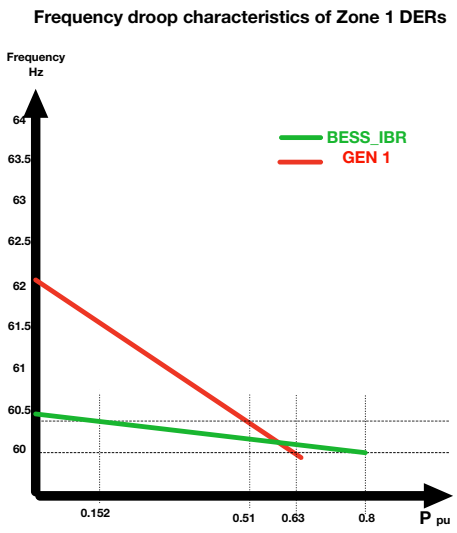

Figure 3.24: Frequency droop characteristics for zone 1 DERs during fault in zone 2.

The transient response of zone 1 DERs is depicted in Figure 3.25. The DERs' active and reactive power are depicted in Figures 3.25a and 3.25b, respectively. As seen from the figures, the active power of the IBRs' response is faster than that of the generator. The BESS instantaneously supplies power after the fault is cleared and supplies power up to its capacity. Figures 3.25c and 3.25d show the transient responses of the DERs to terminal voltage and frequency, respectively. During the fault, the DERs voltage dropped to about 0.15 p.u. and returned to normal values after a slight transient. On the other hand, when the fault occurs, the frequency suddenly falls to 57.6 Hz and fluctuates between 61.4 Hz and 57.6 Hz for a short time. This instantaneous change seems unrealistic, as it is not accompanied by any physical actions. This super-fast frequency oscillation is impossible due to the rotor inertia of synchronous generators. This sudden change in frequency values is the result of the DIgSILENT solver's math.

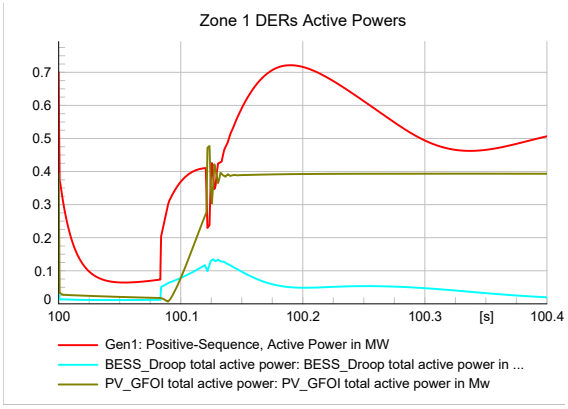

(a) Generators active power transient response.

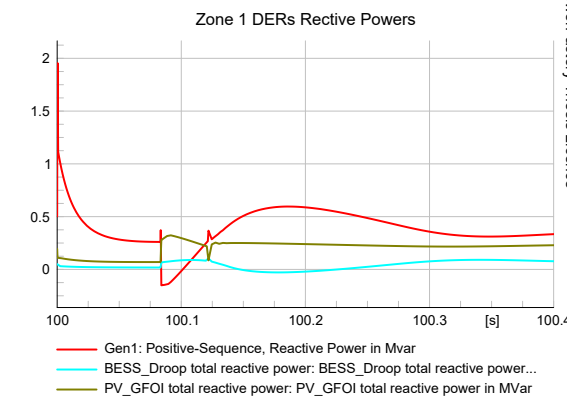

(b) Generators reactive power transient response.

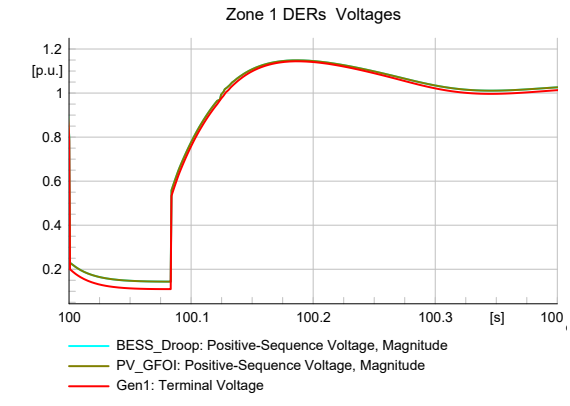

(c) Generators terminal voltages transient response.

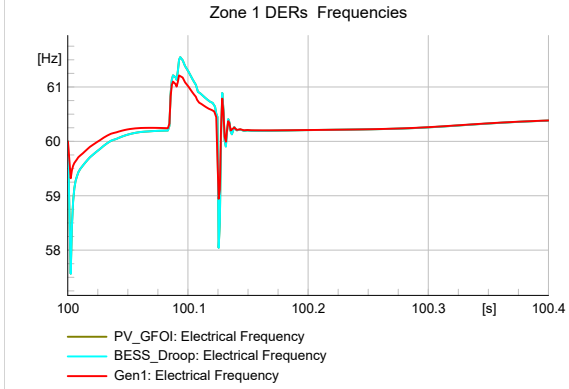

(d) Generators electrical frequencies transient response.

Figure 3.25: Distributed generator transient responses during fault in zone 2.

Finally, Figure 3.26a depicts the zone 1 node voltages and frequencies. Zone 1 node voltages are depicted in Figure 3.26a, whereas the frequencies are depicted in Figure 3.26b. After the fault is cleared, the voltages of zone 1 nodes return to normal values with slight changes in some nodes voltages. The frequencies of zone 1 nodes are almost identical to the generator frequency responses. The microgrid frequency has high fluctuation from 61.4 Hz to 57.6 Hz during transients for the first 50 milliseconds after the fault is cleared, then reaches steady state values within 15 seconds.

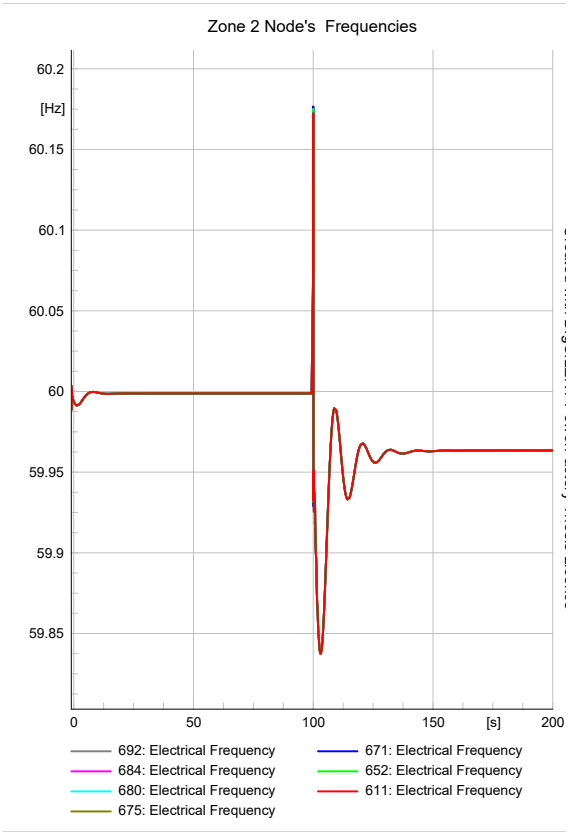

(a) Zone 1 nodes' voltages.

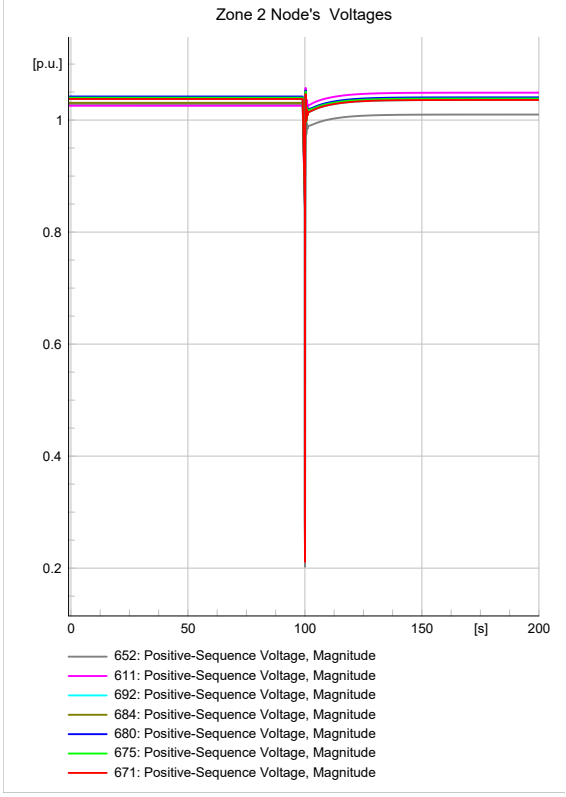

(b) Zone 1 nodes' frequencies.

Figure 3.26: Zone 1 nodes voltages and frequencies.

3.6 Discussion

The proposed protection scheme is applicable to any microgrid that has several distributed energy resources (DREs). This scheme ensures that each protection zone may operate independently of its neighbors' zones or the utility grid. Additionally, because this approach is developed for islanded microgrids, it can be applied to any microgrid that is operated in islanded mode. The proposed protection scheme is applied to the IEEE 13-node microgrid and shows that each protection zone has an adequate generation and load balance. Additionally, the protection system is capable of detecting and isolating just the afflicted

zones in the event of a fault.

Simulating the IEEE 13-node microgrid in the absence of IBRs demonstrates that the proposed protection scheme has a negligible impact. After the fault develops, the microgrid continues to supply the remaining zone with a slight transient.

The penetration of inverter-based resources (IBRs) in microgrids poses significant challenges for microgrid control, particularly for microgrids operating in islanded mode. While the proposed protection scheme works well in with IEEE 13-node microgrid with a low IBR penetration, it has challenges in microgrids with a high IBR penetration or microgrids that are totally powered by IBRs. Thus, to ensure that this protection scheme works in microgrids with high IBR penetration, the microgrid control system should be investigated and improved.

The simulation of the proposed protection scheme's influence on the IEEE-13 microgrid demonstrates that the microgrid's transient reaction is slower in the absence of IBRs than it is with IBRs. In contrast, the effect of IBRs on the microgrid increases the frequency fluctuation during transient response, but the frequency fluctuation of the microgrid in the absence of IBRs is negligible in comparison to the microgrid with IBRs.

Chapter 4

Comparison with Similar Protection Scheme

4.1 Introduction

The fundamental goal of the differential zone protection scheme is to keep the cost of differential protection as minimal as possible. Line current differential protection necessitates the installation of a relay at the end of each line segment in the network, whereas differential zone protection minimizes the number of relays while increasing the protection area. The most effective technique to demonstrate the proposed protection scheme's efficacy is to compare it to other differential zone protection schemes. An engineering design's goal is to reduce system costs while increasing system reliability.

This chapter compares the protection scheme proposed in this thesis to the differential zone protection scheme described by Sortomme et al.[34]. The two protection schemes will be assessed on the same microgrid to provide a fair comparison. The comparison will be made on the basis of the total number of protection devices employed by each scheme and the total number of protection zones contained within each scheme.

4.2 Microgrid Application System

In this comparison, the microgrid application system will be the 18-node distribution network described in [55]. In [31, 56], this 18-node distribution network is converted to a microgrid and modified. The modified 18-node microgrid is illustrated in Figure 4.1 as a single-line diagram.

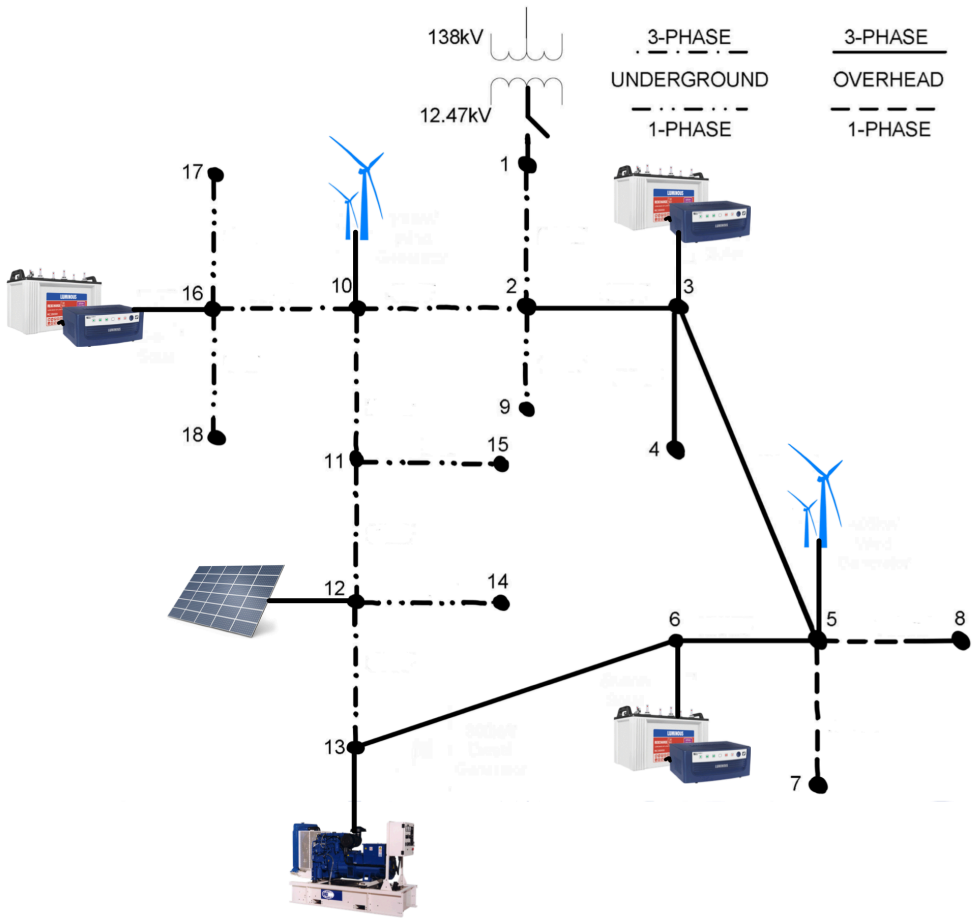

Figure 4.1: 18-node microgrid.

With unbalanced loads, the 18-node network has a total load capacity of 3.03 MVA. With the addition of seven distributed energy resources (DERs), this network is evolved into a

Table 4.1: the 18-node microgrid bus loads and installed capacity.

BUS	Phase A		Phase B		Phase C		Installed capacity
	P (kW)	Q (kVar)	P (kW)	Q (kVar)	P (kW)	Q (kVar)	P(kW)
3	117	73	121	65	90	98	BESS-564
4	97	33	86	35	91	36	
5							Wind-400
6	46	15	77	23	64	19	BESS-564
7	100	65					
8			85	32			
9					354	180	
10							Wind-100
12							PV-564
13	75	34	75	34	75	34	Gen-300
14	111	53					
15					176	34	
16	89	63	89	63	89	63	BESS-564
17			314	126			
18	210	99					
Total	**845**	**435**	**847**	**378**	**939**	**437**	**3056**

microgrid. Three of them are battery energy storage system (BESS), comprising 1692 kW. Additionally, one photovoltaic inverted-base resources (PV-IBRs) is installed with capacity of 564 kW. The microgrid's other two distributed energy resources (DERs) are wind turbine generators with capacities of 100 kW and 400 kW. The microgrid's last DER is a 300 kW diesel generator. The microgrid's bus loads and installed capacity are listed in Table 4.1.

4.3 Proposed Protection Scheme

This section will develop a comprehensive protection system for the 18-node microgrid based on the protection scheme provided in Chapter 2. As previously stated, the proposed protection scheme is based on a five-step graph partitioning algorithm. The microgrid will be partitioned into two sections following these five steps. If the partitioned areas can be further divided, the graph partitioning algorithm can be repeated. Finally, the proposed

protection scheme will be finalized if the divided areas cannot be further divided.

The graph partitioning algorithm will be applied in the prescribed sequence to the 18-node microgrid:

Step 1: Convert the 18-node microgrid into an edge-weighted graph. This step requires the results of the 18-node microgrid lines' power flow. Table 4.2 summarizes the power flow results for the 18-node microgrid lines, and Figure 4.2 illustrates the 18-node microgrid's single line diagram with the power flow results. The graph network of the 18-node microgrid is depicted in Figure 4.3.

Table 4.2: Power flow results for the 18-node microgrid.

Line	**Power flow in MW**
Line 2-3	0.101
Line 2-9	0.354
Line 2-10	0.254
Line 3-4	0.274
Line 3-5	0.146
Load 3	0.328
Line 5-6	0.069
Line 5-7	0.1
Line 5-8	0.085
Line 6-13	0.18
Load 6	0.187
Line 10-11	0.336
Line 10-16	0.183

Table 4.2 continued from previous page

Line	Power flow in MW
Line 11-12	0.512
Line 11-15	0.176
Line 12-13	0.323
Line 12-14	0.111
Load 13	0.225
Line 16-17	0.314
Line 16-18	0.21
Load 16	0.267

Step 2: Calculate the Laplacian matrix Q, as well as its eigenvalues and eigenvectors.

Step 3: Create the partitioning matrix P using the first two eigenvectors of the Laplacian matrix Q.

Step 4: Select seeds for each of the two partitioned areas.

Step 5: Allocate the remaining vertices into the two partitioned areas.

The 18-node microgrid can be separated into two zones using the graph partitioning algorithm. The first zone is limited in size and is served by buses 16, 17, and 18. In comparison to the first zone, the second zone is much larger. Because the first zone contains just one DER, it cannot be subdivided further. On the other hand, the second zone has six DERs, allowing it to be partitioned further.

Now, the second zone will be divided into two sections using the graph partitioning algorithm. The exact five steps will be applied to the second zone as follows:

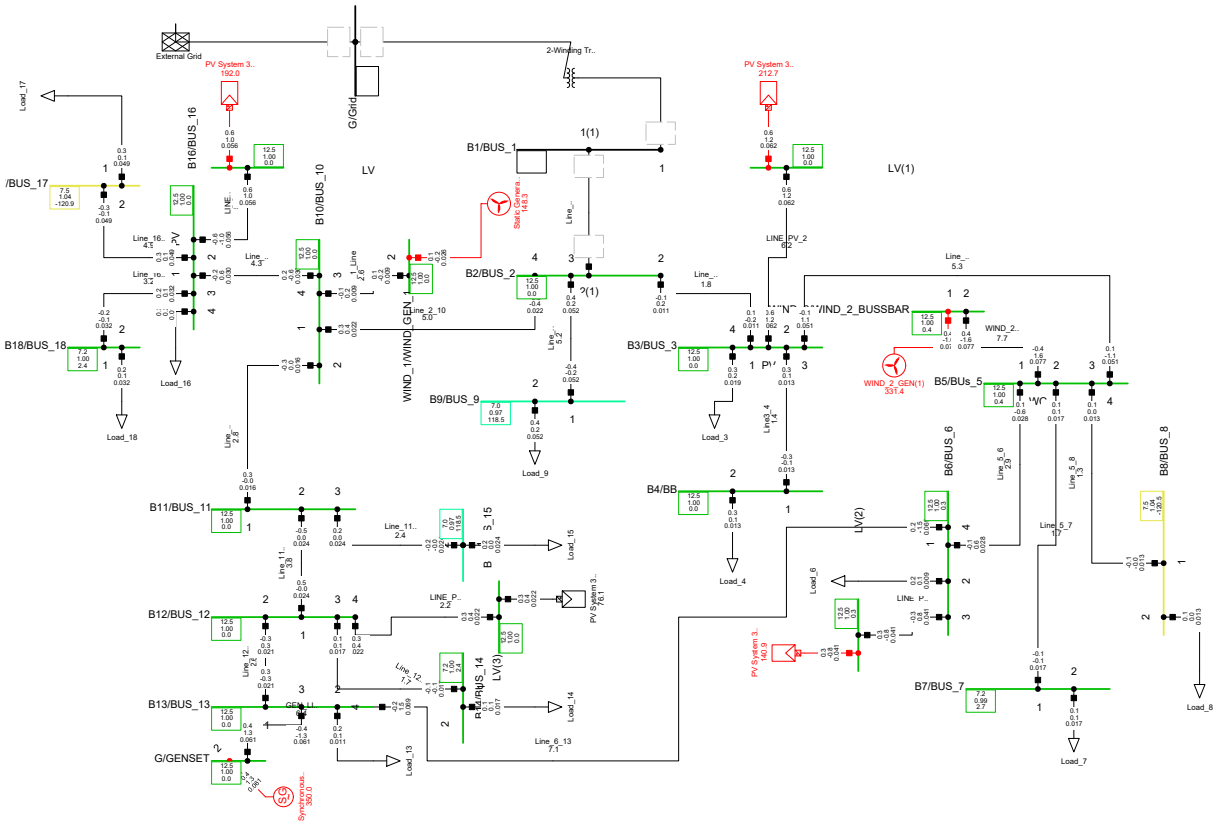

Figure 4.2: 18-node microgrid single-line diagram with powerflow results.

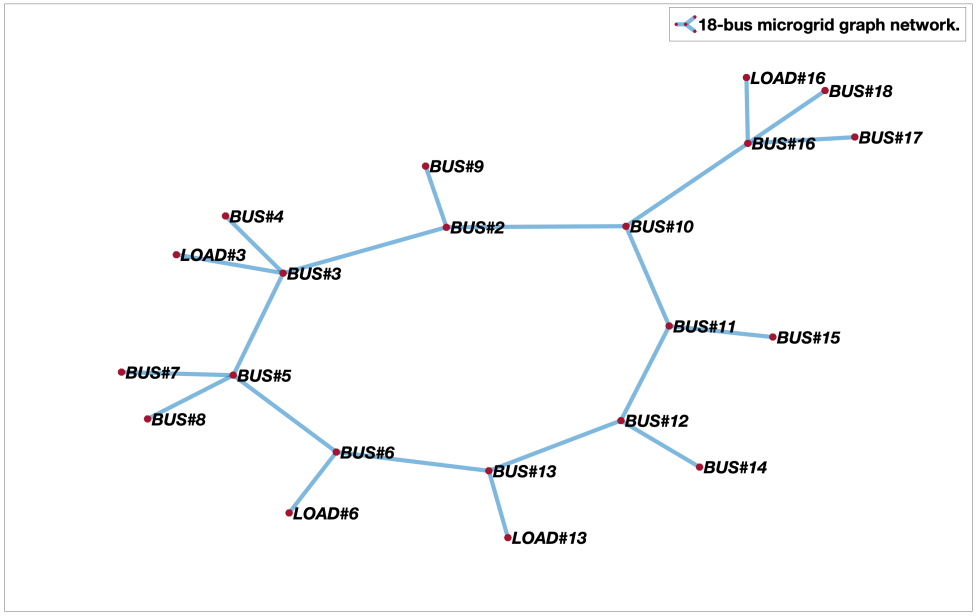

Figure 4.3: 18-node microgrid graph network.

Step 1: Convert the second zone into an edge-weighted graph. This step requires the second zone lines' power flow results. The second zone lines' power flow results are summarized in Table 4.3, and the single line diagram of the second zone with the power flow results is illustrated in Figure 4.4. Figure 4.5 depicts the graph network of the second zone.

Table 4.3: Zone 2 Poweflow results.

Line	**Power flow in MW**
line 2-3	0.062
Line 2-9	0.354
Line 2-10	0.416
Line 3-4	0.274
Line 3-5	0.169

Table 4.3 continued from previous page

Line	Powerflow in MW
Load 3	0.328
Line 5-6	0.046
Line 5-7	0.1
Line 5-8	0.085
Line 6-13	0.158
Load 6	0.187
Line 10-11	0.316
Line 11-12	0.492
Line 11-15	0.176
Line 12-13	0.303
Line 12-14	0.111
Load13	0.225

Step 2: Calculate the Laplacian matrix Q, as well as its eigenvalues and eigenvectors.

Step 3: Create the partitioning matrix P using the first two eigenvectors of the Laplacian matrix Q.

Step 4: Select seeds for each of the two partitioned areas.

Step 5: Allocate the remaining vertices into the two partitioned areas.

Zone 2 could be divided into two zones using the graph partitioning algorithm. The first zone is containing buses 3, 4, 5, 6, 7, and 8 while the second zone contains buses 2, 9, 10, 11, 12, 13, 14, and 15. Both zones contain three DERs, the first zone have total capacity of 1528

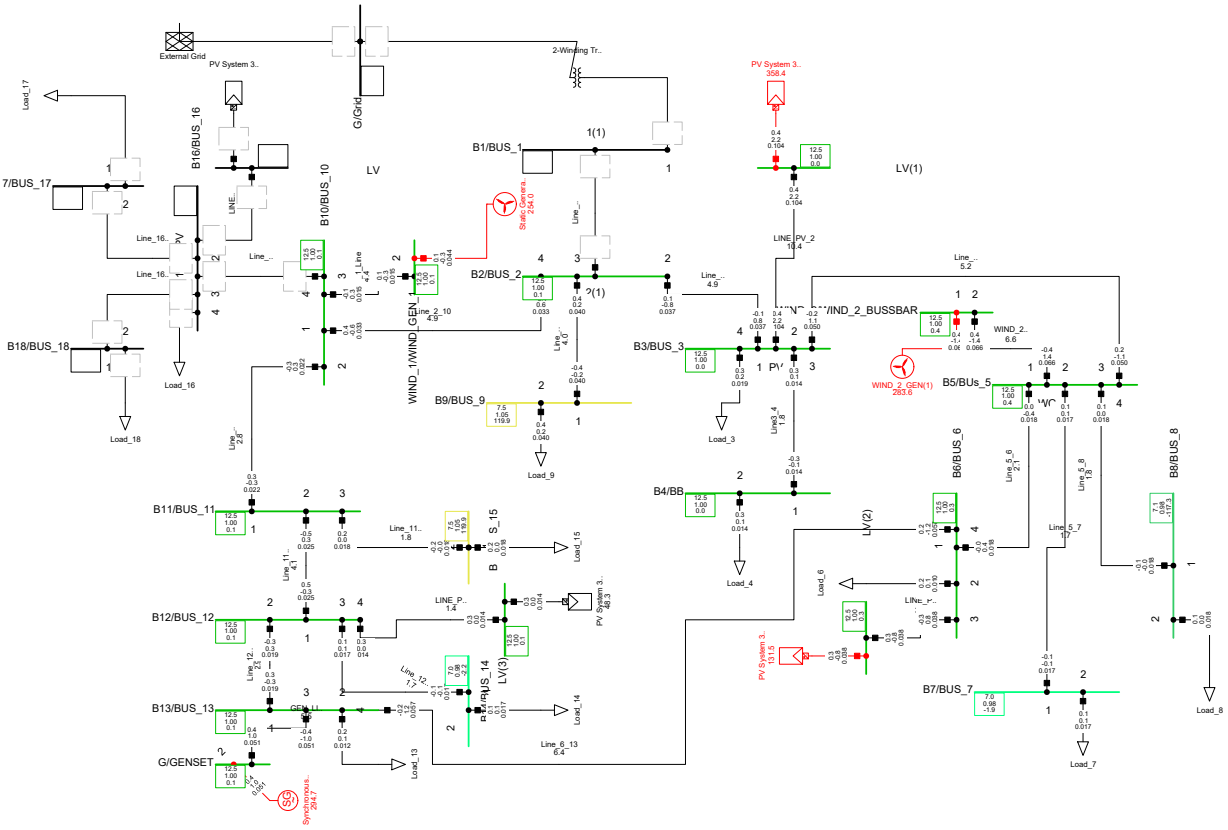

Figure 4.4: Zone 2 single-line diagram with powerflow results.

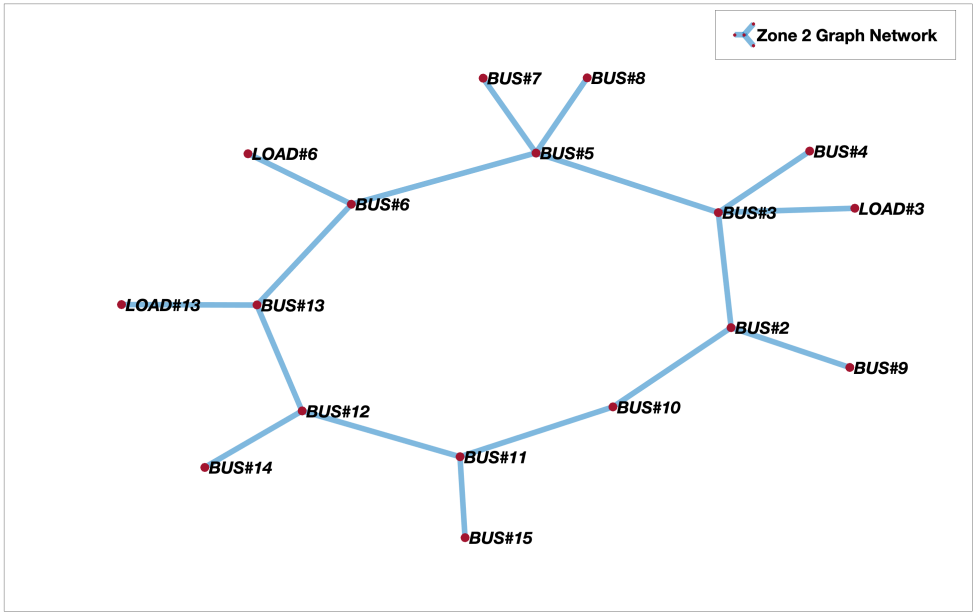

Figure 4.5: Zone 2 graph network.

kW while the second zone have total capacity of 964 kW. The total load in the first zone is 974 kW while the total load in the second zone is 900 kW. As the results demonstrate, the first zone has an adequate generation and load balance and it can be further subdivided. On the other hand, despite the fact that the second zone has nearly attained generation and load balance, further subdivision into additional zones is not feasible due to the location of the DERs.

Now consider zone 3 to be the representation of buses 3, 4, 5, 6, 7, and 8. Zone 3 cannot be subdivided further due to the placement of the wind turbine DER. The wind turbine is installed on bus 5, which is unloaded and located in the middle of zone 3. However, by adding a new bus to connect bus 3 and bus 5 to the wind turbine, zone 3 will gain flexibility. Zone 3 may be further split into two portions based on this idea. The graph partitioning algorithm steps will be applied to zone 3 as follows:

Table 4.4: Zone 3 Power flow results.

Line	Power flow in MW
Line 3-4	0.274
Line 3-WG	0.285
Line WG-5	0.074
Line 5-6	0.111
Line 5-7	0.1
Line 5-8	0.085

Step 1: Convert the zone 3 into an edge-weighted graph. This step requires the results of zone 3 lines' power flow. Table 4.4 summarizes the power flow results for zone 3 lines, and Figure 4.6 illustrates the zone 3 single line diagram with the power flow results. The graph network of zone 3 is depicted in Figure 4.7.

Step 2: Calculate the Laplacian matrix Q, as well as its eigenvalues and eigenvectors.

Step 3: Create the partitioning matrix P using the first two eigenvectors of the Laplacian matrix Q.

Step 4: Select seeds for each of the two partitioned areas.

Step 5: Allocate the remaining vertices into the two partitioned areas.

Finally, the design of the proposed protection scheme for the 18-node microgrid is complete. The graph partitioning algorithm is used to partition the microgrid into four protective zones. The first zone consists of buses 16, 17, and 18 and is equipped with one DER with a total capacity of 564 kW and a total load capacity of 791 kW. The second zone is the largest, consisting of buses 2, 9, 10, 11, 12, 13, 14, and 15, as well as three DERs totaling 964 kW and 866 kW of load capacity. The third zone consists of buses 6, 7, and 8 and is equipped with a single DER with a total capacity of 564 kW and a total load capacity of 374 kW. The last protection zone is comprised of buses 3, 4, and 5, as well as two DERs with a combined capacity of 964 kW and a load capacity of 602 kW.

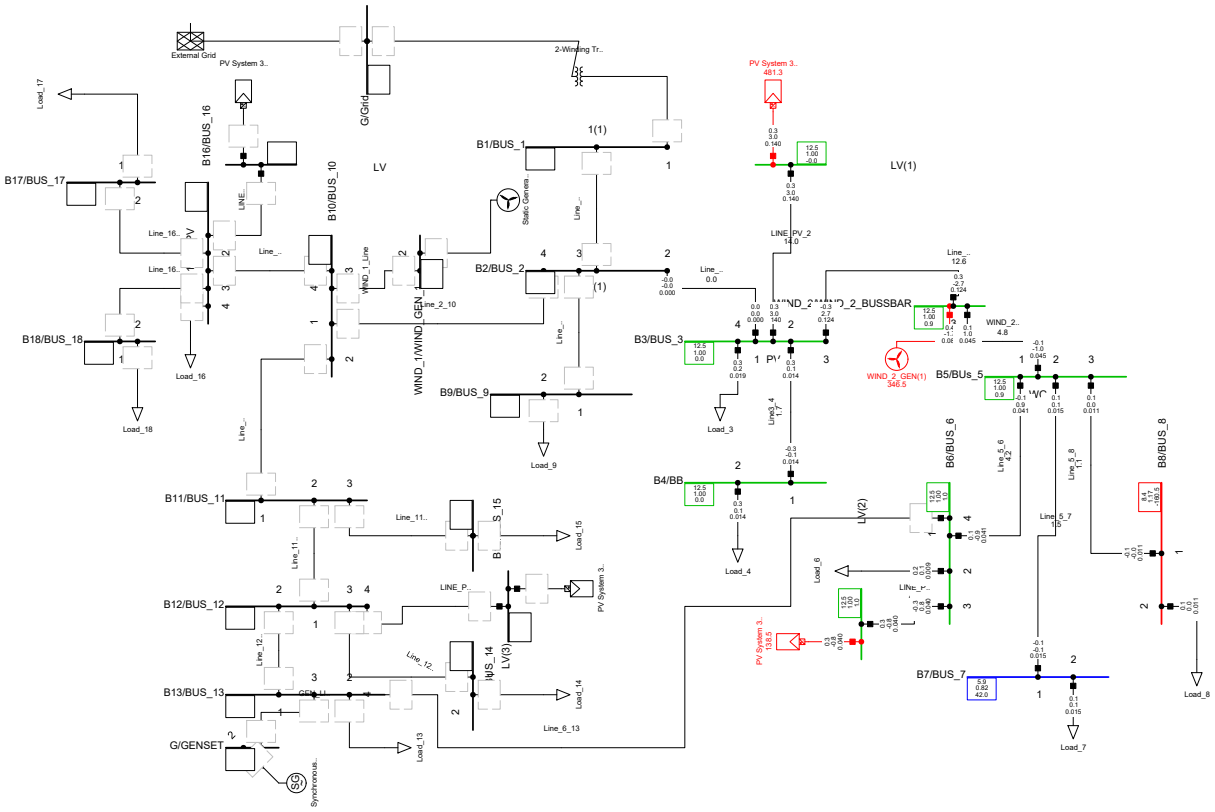

Figure 4.6: Zone 3 single-line diagram with powerflow results.

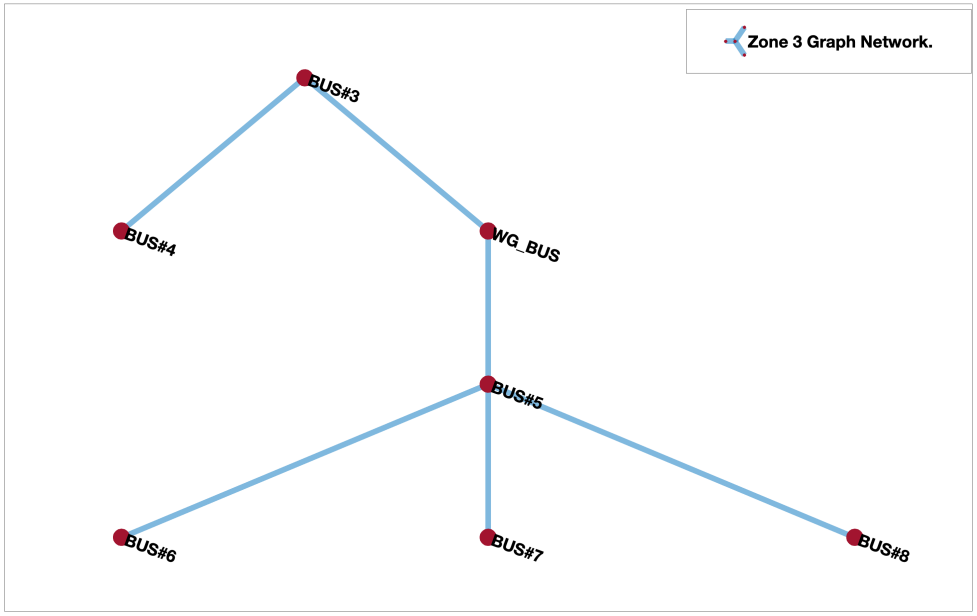

Figure 4.7: Zone 3 graph network.

Eleven buses require the installation of digital relays as part of this protection scheme. Each DER bus, as well as each interconnection bus between zones, will require a digital relay. Buses 2, 5, 13, and 16 serve as interconnections buses. On the other hand, the necessary number of smart current sensors is equal to the number of loaded buses. That is, a sensor must be installed on each of 12 buses. Due to the imbalanced nature of the microgrid and the fact that some loads are single-phase, the smart current sensors employed in this system will be single-phase. This technique will utilize a total of 22 single-phase sensors. The digital relays will likewise be single-phase devices; consequently, this design will utilize a total of 33 single-phase digital relays. The proposed protection scheme for the 18-node microgrid is summarized in Table 4.5.

The protective zones should be somewhat modified, particularly zone 1 and zone 2. This change aims to maintain the generation and load balance and connect zone 1 to many zones.

Table 4.5: Proposed protection scheme for the 18-node microgrid summary.

	Zone 1	**Zone 2**	**Zone 3**	**Zone 4**
Buses	16, 17, and 18	2, 9, 10, 11, 12, 13, 14, and 15	6, 7, and 8	3, 4, and 5
Generation sources	One	Three	One	Two
Installed capacity	564 kW	964 kW	564 kW	964 kW
Load consumption	791 kW	866 kW	374 kW	602 kW
Digital relays 1-PH	33 single-phase relay			
Smart current sensors 1-PH	22 single-phase sensor			

Table 4.6: The modified protection scheme for the 18-node microgrid summary.

	Zone 1	**Zone 2**	**Zone 3**	**Zone 4**
Buses	10, 16, 17, and 18	11, 12, 13, 14, and 15	6, 7, and 8	2, 3, 4, 5, and 9
Generation sources	Two	Two	One	Two
Installed capacity	664 kW	864 kW	564 kW	964 kW
Load consumption	791 kW	512 kW	374 kW	956 kW
Digital relays 1-PH	33 single-phase relay			
Smart current sensors 1-PH	22 single-phase sensor			

Buses 2 and 10 are unloaded; also, bus 10 is equipped with a wind turbine DER. The issue occurs with bus 9, which is equipped with a total load capacity of 354 kW. Thus, zone 1 will include bus 10, while zone 4 will have buses 2 and 9. Zone 1 will now have a total capacity of 664 kW and a total load capacity of 791 kW as a result of this alteration. Zone 1 remains without a generation and load balance, but it is now connected to zones 2 and 4. If a fault occurs in the microgrid, just the faulty zone will be isolated, while the remaining zones will function as a single microgrid. As a result, zone 1 will receive the required power from the DERs in the other zones. The revised protection scheme for the 18-node microgrid is summarized in Table 4.6.

4.4 Previous Differential Zone Protection Scheme

There are a few protection schemes that are based on the concept of differential zones. E. Sortomme et al. Sortomme et al.[34] proposed a differential zone protection scheme, and S. Venkata et al. modified the method [5]. This is an innovative and new approach to

microgrid protection. The microgrid might be divided into small islands, with each island having its own differential zone protection scheme. The differential zones will be defined following the use of an optimum relay placement formulation. The genetic algorithm [57] is used to minimize the total investment cost of the protection devices and the cost of customer interruption over a certain time period.

This protection scheme is applied to the 18-node microgrid shown in Figure 4.1, assuming that 10% of the time, the microgrid is in islanded mode. The load on bus 4 is considered a critical load in this study, whereas the remaining loads are considered normal residential loads. Additionally, it is assumed that each phase would require its own protection device. Thus, the optimization problem is performed on a per-phase basis. The microgrid is divided into small single-phase islands, each with its own protection scheme with single-phase differential zones.

The microgrid consists of two distinct differential zones. Buses 1, 2, 3, 4, 6, 9, and 10-18 are located in the first zone, whereas buses 3, 4, 5, 6, 7, and 8 are located in the second zone. Due to the crucial nature of the load on bus 4, buses 3 and 4 operate in both zones. Phases A and B have zone boundaries at buses 3 and 6, whereas phase C has zone boundaries at buses 3 and 5. Each phase includes 11 digital relays, whereas phases A, B, and C have 4, 3, and 3 smart current sensors, respectively. This scheme utilizes a total of 33 digital relays and 10 smart current sensors. The differential zone protection scheme proposed in [34] is summarized in Table 4.7.

4.5 Comparison

Finally, after implementing both protection schemes on the same microgrid, a comparison of the two protection schemes is performed. The two protection schemes will be evaluated

Table 4.7: summary of the differential zone protection scheme.

	Zone 1	**Zone 2**
Buses	1, 2, 3, 4, 6, 9, and 10-18	3, 4, 5, 6, 7, and 8
Generation sources	Six	Three
Installed capacity	2656 kW	1528 kW
Load consumption	2446 kW	1074 kW
Digital relays 1-PH	33 single-phase relay	
Smart current sensors 1-PH	10 single-phase sensor	

Table 4.8: Comparison between the two differential protection schemes.

	PPS in this thesis	**PPS in [34]**
Protection zones	Four	Two
Digital relays 1-PH	33	33
Smart current sensors 1-PH	22	10

in terms of total protection zones and total protective devices used.

The protection scheme described in this thesis results in the division of the 18-node microgrid into four protection zones. Each zone is linked to the other two, preventing the unfaulted zone from working in a solitary state. When a fault occurs, only the fault zone is isolated; the remaining zones operate as a single huge island. On the other hand, the proposed protection scheme in [34] results in the 18-node microgrid being divided into two large zones with some overlapped buses. The overlapped buses enhanced generation in the two zones and aided in balancing the generation and load in the protection zones.

On the other aspect of this comparison, the total number of digital relays and smart current sensors used in the proposed protection scheme in this thesis is 33 relays and 22 sensors, while the protection scheme proposed in [34] used 33 relays and 10 sensors. The proposed protection scheme in this thesis uses 12 smart current sensors more with an increase of 15.7% in the total investment cost for the protection devices. Table 4.8 summarizes the comparison between the two protection schemes.

4.6 Discussion

The proposed protection scheme in this thesis is based on the graph partitioning algorithm. This algorithm is heavily dependent on the power flow results; therefore, the protection zones may vary depending on the power flow results. As a result, the design of this protection system is reliant on the microgrid DERs' power dispatch; altering the power dispatch of the DERs results in an alteration of the protection zones. On the other hand, this protection scheme takes the generation and load balance into consideration. Thus, this protection scheme could be applied to an islanded microgrid.

The differential zone protection scheme proposed in[34] is based on an optimization problem. The relay is positioned using a genetic algorithm in this optimization problem. The overall investment cost of the protective devices and the cost of customer interruption are the constraints on this optimization problem. Although the 18-node microgrid's results indicate that each protection zone has a sufficient generation to load ratio, the protection scheme did not assure generation and load balance. As a result, this protection scheme does not guarantee that the microgrid can be operated completely autonomously in an islanded microgrid. Additionally, the findings from the 18-node microgrid demonstrate that this approach maximizes the benefits of DERs by overlapping them into different protective zones.

When the two protection schemes are compared, it is clear that the proposed protection scheme in this thesis has more protection zones than the protection scheme in [34]. The addition of protective zones improves the microgrid's reliability and lowers the cost of customer interruption. On the other hand, the protection scheme described in this thesis employs more protective devices, resulting in a 15.7 % increase in the total investment cost.

Chapter 5

Conclusion and Future Work

Microgrid protection is a critical challenge for microgrid implementations, particularly for islanded microgrids. The differential zone protection scheme suggested in this thesis is intended for use in both islanded and grid-connected microgrids. The protection zones in this scheme are carefully determined using a graph partitioning algorithm to guarantee that each zone has an adequate generation and load balance. As a result, when a fault develops in the microgrid, only the faulty zone is isolated, while the remaining zones operate as a single large zone with enough generation and load balance.

The proposed protection scheme is simulated with an IEEE 13-node microgrid and demonstrates that each protection zone had a sufficient generation and load balance and that the protection system is capable of detecting and isolating only the affected zones in the event of a fault. Additionally, the proposed protective scheme's impact on the same microgrid is modelled using DIgSILENT PowerFactory software in two scenarios with and without IBRs. The increasing penetration of inverter-based resources (IBRs) in microgrids may create significant control issues, particularly for islanded microgrids. While the proposed protection scheme works well with IEEE 13-node microgrid with a low IBR penetration, it has challenges in microgrids with a high IBR penetration or microgrids that are totally powered by IBRs. Thus, to ensure that this protection scheme works in microgrids with high IBR penetration, the microgrid control system should be investigated and improved.

On the other hand, although that the proposed protection scheme accomplished its

objective, it is not without limitations and practical drawbacks. The proposed scheme's graph partitioning algorithm is highly dependent on the power flow results. Therefore, if the power flow results change due to installing or removing DERs, the generation and load balance may not be maintained. Additionally, the differential protection scheme is communication-dependent; consequently, communication failures can significantly influence this protection scheme.

Due to the high reliance on power flow results in this protection scheme, it is necessary to adapt it to ensure generation and load balance in the event that any of the DERs is de-energized or in the case of a networked microgrid. The protective zones must be reconfigured after every update to the microgrid. Additionally, a microgrid cyber-physical model is required to validate the communication system's connection to the power system. Additionally, the protection scheme should include fault location and restoration systems to precisely locate and restore faulted lines. Finally, the microgrid control system should be investigated and improved to guarantee that this protection scheme is applicable in microgrids with high penetration of IBRs.

Appendices

Appendix A

PPS Example

This section illustrates in detail how to implement the proposed protection scheme on an electric network. The IEEE 9-node is a small network with three generators, three transformers, nine buses, and six lines. This example demonstrates how the proposed protection scheme may be applied to the IEEE 9-node network.

Two steps are required to apply the proposed protection scheme to any network. The first step is to do a network power flow study. The second step is to split the network into two zones using the graph partitioning algorithm. Following these steps, a feasibility check is conducted to see whether the split zones can be further divided into two zones.

Figure A.1 illustrates the power flow analysis of the IEEE 9-node network. Power flow between the busses is required by the graph partitioning algorithm. Thus, this network could be reduced to a six-node network. Figure A.2 depicts a simplified six-node network with power flow results, while Table A.1 depicts the power flow in each line.

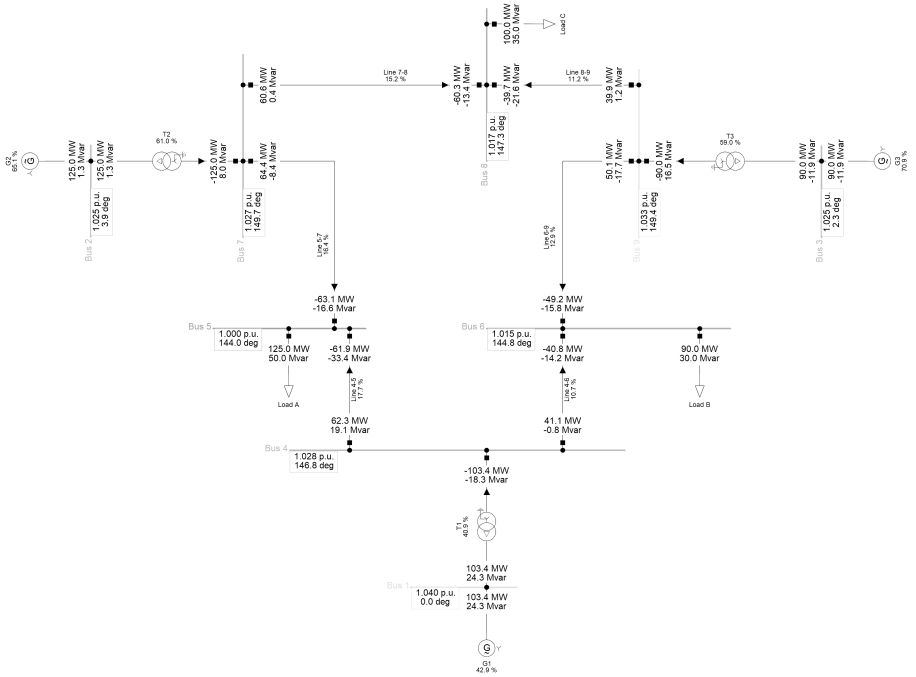

Figure A.1: IEEE 9-node network with powerflow results.

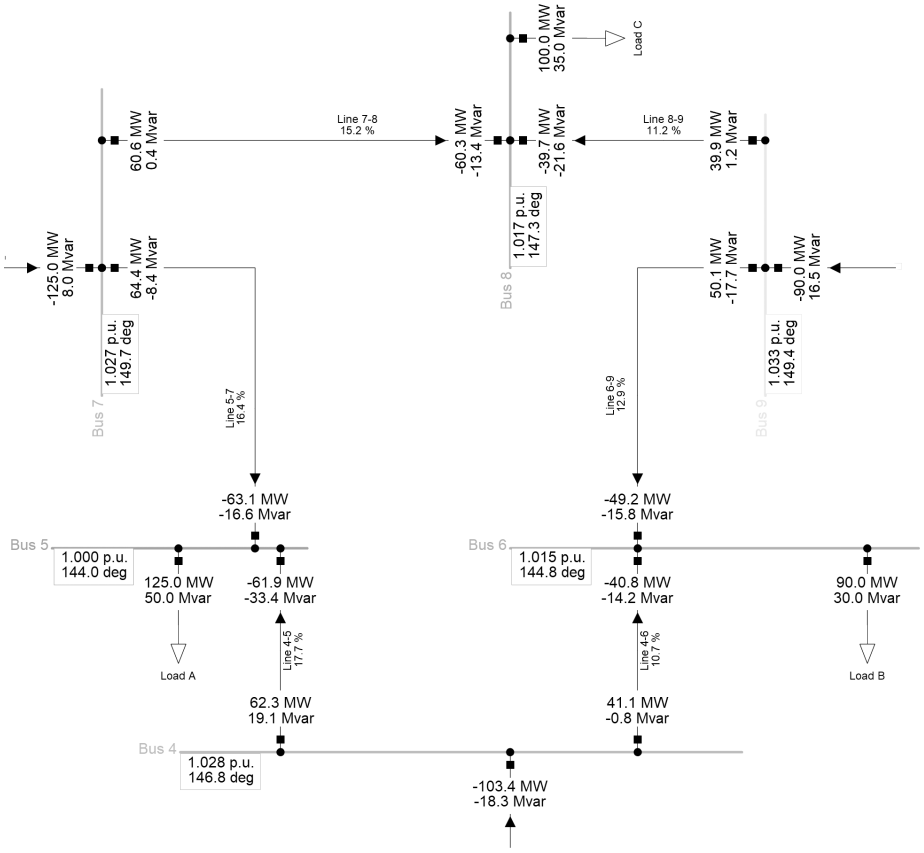

Figure A.2: Simplified 6-node Network with powerflow results.

Table A.1: IEEE 9-node Network Lines power flow.

Line	Power flow in MW
Line 4-5	62.3
Line 4-6	41.4
Line 5-7	64.4
Line 6-9	50.1
Line 7-8	60.6
Line 8-9	39.9

The second part in implementing the proposed protection scheme is to segment the network. This part will be carried out using the graph partitioning algorithm. Section 2.3 of this thesis delves deeply into the algorithm; five steps comprise the algorithm. Converting the simplified six-node network to an edge-weighted graph G is the first step. The simplified

six-node network's graph network is depicted in Figure A.3.

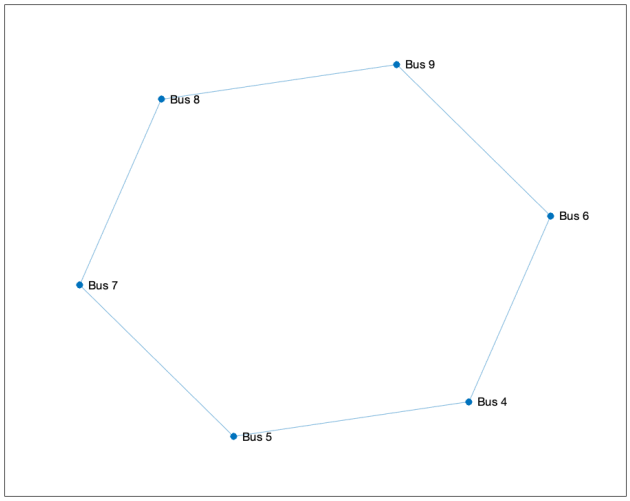

Figure A.3: Simplified 6-node Graph Network.

The graph partitioning algorithm second step is to compute the Laplacian matrix Q, as well as its eigenvalues and related eigenvectors. This step requires the adjacency matrix A and the degree matrix D to be computed. Below are the adjacency matrix and degree matrix D.

$$A = \begin{bmatrix} 0 & 62.3 & 41 \cdot 1 & 0 & 0 & 0 \\ 62 \cdot 3 & 0 & 0 & 64 \cdot 4 & 0 & 0 \\ 41 \cdot 1 & 0 & 0 & 0 & 0 & 50.1 \\ 0 & 64.4 & 0 & 0 & 60.6 & 0 \\ 0 & 0 & 0 & 60.6 & 0 & 39 \cdot 9 \\ 0 & 0 & 50 \cdot 1 & 0 & 39 \cdot 9 & 0 \end{bmatrix} \tag{A.1}$$

$$D = \begin{bmatrix} 2 & 0 & 0 & 0 & 0 & 0 \\ 0 & 2 & 0 & 0 & 0 & 0 \\ 0 & 0 & 2 & 0 & 0 & 0 \\ 0 & 0 & 0 & 2 & 0 & 0 \\ 0 & 0 & 0 & 0 & 2 & 0 \\ 0 & 0 & 0 & 0 & 0 & 2 \end{bmatrix} \tag{A.2}$$

The Laplacian matrix can be determined by subtracting the adjacency matrix A from the degree matrix D after computing these two matrices.

$$Q = D - A \tag{A.3}$$

$$Q = \begin{bmatrix} 2 & -62.3 & -41 \cdot 1 & 0 & 0 & 0 \\ -62 \cdot 3 & 2 & 0 & -64 \cdot 4 & 0 & 0 \\ -41 \cdot 1 & 0 & 2 & 0 & 0 & -50.1 \\ 0 & -64.4 & 0 & 2 & -60.6 & 0 \\ 0 & 0 & 0 & -60.6 & 2 & -39 \cdot 9 \\ 0 & 0 & -50 \cdot 1 & 0 & -39 \cdot 9 & 2 \end{bmatrix} \tag{A.4}$$

After obtaining the Laplacian matrix, it is possible to extract the eigenvalues and related eigenvectors. Below are presented the eigenvalue vector λ and the eigenvector matrix V.

$$\lambda = \begin{bmatrix} \lambda_1 \\ \lambda_2 \\ \lambda_3 \\ \lambda_4 \\ \lambda_5 \\ \lambda_6 \end{bmatrix} = \begin{bmatrix} -180.0764 \\ -52.0281 \\ -47 \cdot 5619 \\ 51.5619 \\ 56.0281 \\ 112.0764 \end{bmatrix} \tag{A.5}$$

$$V = \begin{bmatrix} 1.00 & 0.1892 & 1.4393 & -1.4393 & 0.1892 & -1.00 \\ 1.3258 & -0.8518 & 0.7901 & 0.7901 & 0.8518 & 1.3258 \\ 0.6686 & 1.5398 & 0.5380 & 0.5380 & -1.5398 & 0.6686 \\ 1.2987 & -0.8976 & -0.7843 & 0.7843 & -0.8976 & -1.2987 \\ 0.9501 & 0.1049 & -1.4811 & -1.4811 & 0.1049 & 0.9501 \\ 0.6487 & 1.5053 & -0.6486 & 0.6486 & 1.5053 & -0.6487 \end{bmatrix} \tag{A.6}$$

The third step is to create the partitioning matrix P from the Laplacian matrix Q's first two eigenvectors. Below are the first two eigenvectors of the Laplacian matrix Q, $X = [x_1 x_2]$.

$$X = \begin{bmatrix} 1.00 & 0.1892 \\ 1.3258 & -0.8518 \\ 0.6686 & 1.5398 \\ 1.2987 & -0.8976 \\ 0.9501 & 0.1049 \\ 0.6487 & 1.5053 \end{bmatrix} \tag{A.7}$$

The partitioning matrix $\widehat{P} = N(X)XX^T N(X)$ where $N(X)$ is a diagonal matrix with $n_{ii} = 1/\sqrt{\sum_{h=1}^{k} x_{ih}'^2}$. n_{ii} is the reciprocal of the norm of row i of X.

Another approach is to use the following formula to determine the partitioning matrix.

$$\widehat{P}_{ij} \quad = \quad x_i'^T x_j' / \left(\|x_i'\| \left\|x_j'\right\| \right) \tag{A.8}$$

The simplified six-node network's partitioning matrix is given below.

$$\widehat{P} = \begin{bmatrix} 1.00 & 0.7262 & 0.5619 & 0.7026 & 0.9970 & 0.5596 \\ 0.7262 & 1.00 & -0.1607 & 0.9994 & 0.7769 & -0.1634 \\ 0.5619 & -0.1607 & 1.00 & -0.1939 & 0.4966 & 1.00 \\ 0.7026 & 0.9994 & -0.1939 & 1.00 & 0.7553 & -0.1966 \\ 0.9970 & 0.7769 & 0.4966 & 0.7553 & 1.00 & 0.4942 \\ 0.5596 & -0.1634 & 1.00 & -0.1966 & 0.4942 & 1.00 \end{bmatrix} \tag{A.9}$$

The cosine of the angle between the row vertices i and j of matrix X is the $\widehat{P}_{ij}$ element of the partitioning matrix. These directional cosines indicate the proximity of the vertices to one another.

The fourth step is to choose two vertices to act as the dividing areas' seeds. The initial seed will be randomly chosen. The second seed must ensure that the partitioning vector elements $\widehat{P}_{i1}$ is minimized.

If the first seed is vertex one, the second seed must ensure that the $\widehat{P}_{ij}$ element is minimized.

Below is the first column of the partitioning matrix $\widehat{P}_{ij}$.

$$\widehat{P_{i1}} = \begin{bmatrix} 1.00 \\ 0.7262 \\ 0.5619 \\ 0.7026 \\ 0.9970 \\ 0.5596 \end{bmatrix} \tag{A.10}$$

The element $\widehat{P}_{61} = 0.5596$ is the minimum cosine of the angle between vertex one and the other vertices. Then vertex 6 is the second seed for area two. vertex 1 corresponds to bus-4, whereas vertex 6 corresponds to bus-9.

Columns 1 and 6 of the partitioning matrix are required to solve for the remaining vertices. As illustrated below, the partitioning matrix $\widehat{P_s}$ contains only the seeds vertices column.

$$\widehat{P_s} = \begin{bmatrix} 1.00 & 0.5596 \\ 0.7262 & -0.1634 \\ 0.5619 & 1.00 \\ 0.7026 & -0.1966 \\ 0.9970 & 0.4942 \\ 0.5596 & 1.00 \end{bmatrix} \tag{A.11}$$

The last step is to determine if the remaining vertices are near to the seed, the matrix $\widehat{P_s}$'s

two columns will be subtracted.

$$\widehat{P_{1-6}} = \begin{bmatrix} 0.4404 \\ 0.8896 \\ -0.4381 \\ 0.8892 \\ 0.5029 \\ -0.4404 \end{bmatrix} \tag{A.12}$$

If the row index i is positive for any of the remaining vertices, this vertex will be in the area containing the seed vertex 1; if it is negative, this vertex will be in the area containing the seed vertex 6.

Subtracting column 6 from column 1 of the partitioning matrix $\widehat{P}$ reveals that rows 1,2,4, and 5 have positive values, whilst rows 3,and 6 contain negative values. Thus, area one has the vertices 1,2,4, and 5 whereas area two contains the vertices 3, and 6. In Area 1, the equivalent buses are "Bus 4, Bus 5, Bus 7, Bus 8," whereas in Area 2, the corresponding buses are "Bus 6, Bus 9." The partitioned areas, corresponding buses, generation sources, total generation capacity, and loads are shown in Table A.2.

Table A.2: First Partitioned areas.

	Area 1	Area 2
Busses	Bus 6, Bus 9	Bus 4, Bus 5, Bus7, and Bus8
Number of Sources	1	2
Installed capacity in MW	108.8	410.7
Load consumption in MW	90	225

Area 1 is comprised of two buses, bus 6 and bus 9, and is served by a single generating source. Thus, area 1 cannot be subdivided further into two areas.

On the other side, area 2 is comprised of buses 4, 5, 7, and 8, and is served by two generating sources. Additionally, area 2 has an adequate generation capacity. Thus, area 2 may be subdivided into two sections.

Area 2 could be subdivided into two smaller sections. For area 2, the entire partitioning procedure will be repeated. Figures A.4 and A.5 illustrate the power flow and graph network for area 2.The power flow in each line of area 2 is depicted in Table A.3.

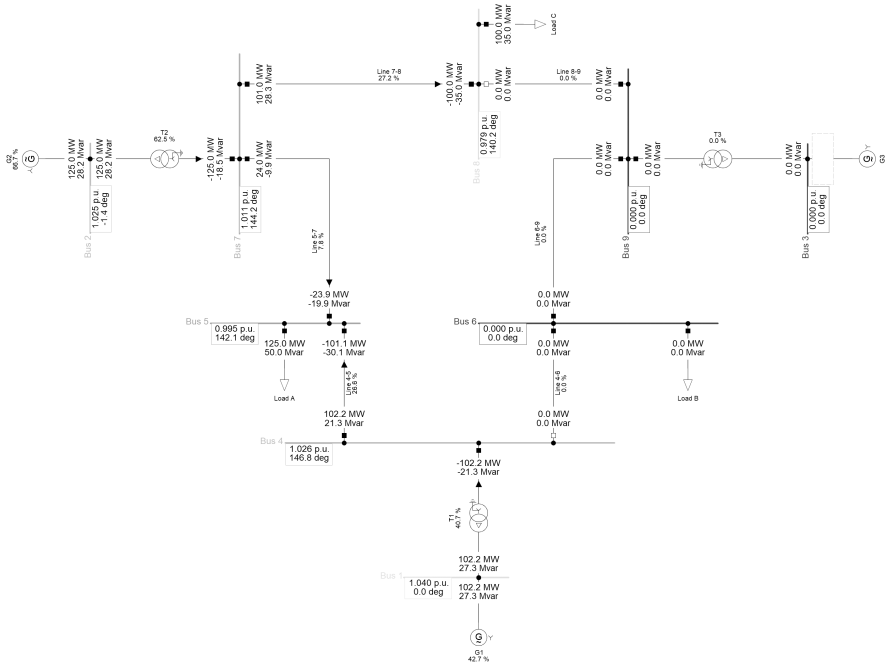

Figure A.4: Area 2 Network powerflow results.

Table A.3: Area 2 Lines power flow.

Line	Power flow in MW
Line 4-5	102.2
Line 5-7	24
Line 7-8	101

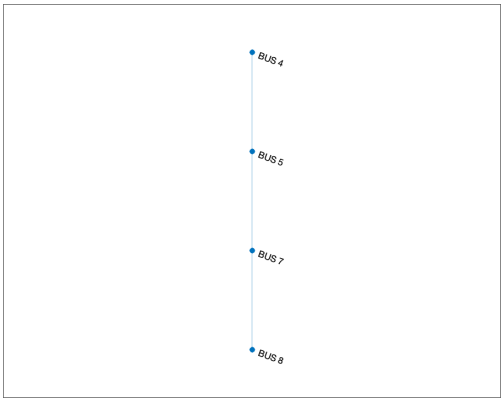

Figure A.5: Area 2 Graph Network.

After performing all of the graph partitioning algorithm steps on area 2, it was possible to divide it into two smaller areas. Buses 4 and 5 are located in Area 21, whereas buses 7 and 8 are located in Area 22. Each of the new two areas has a single generation source, and hence cannot be subdivided further.

Finally, the IEEE 9-node network could be partitioned into three protection zones. This network can now be subjected to the proposed protection scheme. Six digital relays and three smart current sensors are required for the proposed protection scheme. Each generator bus and each zone interconnection bus will be equipped with digital relays. Buses 5, 6, and 8 serve as zones connectivity buses. At each load bus, smart current sensors will be installed. The proposed protection scheme is summarized in Table A.4.

Table A.4: Example Summary

	Zone 1	Zone 2	Zone 3
Busses	Bus 1, Bus 4, and Bus 5	Bus 2, Bus 7, and Bus 8	Bus 3, Bus 6, and Bus 9
Generation sources	One	One	One
Installed capacity	247.5 MW	163.2 MW	108.8 MW
Load consumption	125 MW	100 MW	90 MW
Digital relays	Six		
Smart current sensors	Three		

Bibliography

[1] M. Soshinskaya, W. H. Crijns-Graus, J. M. Guerrero, and J. C. Vasquez, "Microgrids: Experiences, barriers and success factors," *Renewable and Sustainable Energy Reviews*, vol. 40, pp. 659–672, 2014.

[2] M. J. Reno, S. Brahma, A. Bidram, and M. E. Ropp, "Influence of inverter-based resources on microgrid protection: part 1: Microgrids in radial distribution systems," *IEEE Power and Energy Magazine*, vol. 19, no. 3, pp. 36–46, 2021.

[3] D. Lagos, V. Papaspiliotopoulos, G. Korres, and N. Hatziargyriou, "Microgrid protection against internal faults: Challenges in islanded and interconnected operation," *IEEE Power and Energy Magazine*, vol. 19, no. 3, pp. 20–35, 2021.

[4] S. Manson and E. McCullough, "Practical microgrid protection solutions: Promises and challenges," *IEEE Power and Energy Magazine*, vol. 19, no. 3, pp. 58–69, 2021.

[5] S. Venkata, M. Reno, W. Bower, S. Manson, J. Reilly, and G. Jr, "Microgrid protection: Advancing the state of the art," 03 2019.

[6] R. Lasseter, "Microgrids," in *2002 IEEE Power Engineering Society Winter Meeting. Conference Proceedings (Cat. No.02CH37309)*, vol. 1, pp. 305–308 vol.1, 2002.

[7] R. Lasseter and P. Paigi, "Microgrid: A conceptual solution," in *2004 IEEE 35th Annual Power Electronics Specialists Conference (IEEE Cat. No.04CH37551)*, vol. 6, pp. 4285–4290 Vol.6, 2004.

[8] N. Hatziargyriou, H. Asano, R. Iravani, and C. Marnay, "Microgrids," *IEEE Power and Energy Magazine*, vol. 5, no. 4, pp. 78–94, 2007.

[9] K. A. Schwaegerl C, Tao L, Lopes J, Madureira A, Mancarella P, Anastasiadis A, Hatziargyriou N, "Advanced architectures and control concepts for more microgrids," tech. rep., 2009.

[10] S. Parhizi, H. Lotfi, A. Khodaei, and S. Bahramirad, "State of the art in research on microgrids: A review," *IEEE Access*, vol. 3, pp. 890–925, 2015.

[11] A. Cagnano, E. De Tuglie, and P. Mancarella, "Microgrids: Overview and guidelines for practical implementations and operation," *Applied Energy*, vol. 258, p. 114039, jan 2020.

[12] D. T. Ton and M. A. Smith, "The U.S. department of energy's microgrid initiative," *The Electricity Journal*, vol. 25, pp. 84–94, oct 2012.

[13] C. Marnay, S. Chatzivasileiadis, C. Abbey, R. Iravani, G. Joos, P. Lombardi, P. Mancarella, and J. von Appen, "Microgrid evolution roadmap," in *2015 International Symposium on Smart Electric Distribution Systems and Technologies (EDST)*, pp. 139–144, IEEE, sep 2015.

[14] A. Hirsch, Y. Parag, and J. Guerrero, "Microgrids: A review of technologies, key drivers, and outstanding issues," *Renewable and Sustainable Energy Reviews*, vol. 90, pp. 402–411, 2018.

[15] F. Tuffner, T. Williams, K. Schneider, M. Elizondo, Y. Sun, C. C. Liu, Y. Xu, and S. N. G. Gourisetti, "Improving distribution resiliency with microgrids and state and parameter estimation," tech. rep., 01 2015.

[16] Y. Xu, C. C. Liu, K. P. Schneider, and D. T. Ton, "Toward a resilient distribution system," in *2015 IEEE Power Energy Society General Meeting*, pp. 1–5, IEEE, jul 2015.

[17] C. Chen, J. Wang, F. Qiu, and D. Zhao, "Resilient distribution system by microgrids formation after natural disasters," *IEEE Transactions on Smart Grid*, vol. 7, pp. 958–966, mar 2016.

[18] C. Chen and B. Chen, "Modernizing distribution system restoration to achieve resiliency against extreme weather events," in *2018 IEEE Global Conference on Signal and Information Processing (GlobalSIP)*, vol. 105, pp. 895–896, IEEE, nov 2018.

[19] S. Horowitz and A. Phadke, *Power system relaying*. Chichester, West Sussex: John Wiley and Sons, nv - 1 o ed., 2014.

[20] H. Nikkhajoei and R. H. Lasseter, "Microgrid protection," in *2007 IEEE Power Engineering Society General Meeting*, vol. 105, pp. 1–6, IEEE, jun 2007.

[21] A. Hooshyar and R. Iravani, "Microgrid protection," *Proceedings of the IEEE*, vol. 105, no. 7, pp. 1332–1353, 2017.

[22] D. Liu, D. Tzelepis, and A. Dysko, "Protection of microgrids with high amounts of renewables: Challenges and solutions," in *2019 54th International Universities Power Engineering Conference (UPEC)*, pp. 1–6, IEEE, sep 2019.

[23] A. A. Memon and K. Kauhaniemi, "A critical review of AC microgrid protection issues and available solutions," *Electric Power Systems Research*, vol. 129, pp. 23–31, dec 2015.

[24] S. A. Gopalan, V. Sreeram, and H. H. Iu, "A review of coordination strategies and protection schemes for microgrids," *Renewable and Sustainable Energy Reviews*, vol. 32, pp. 222–228, apr 2014.

[25] B. J. Brearley and R. R. Prabu, "A review on issues and approaches for microgrid protection," *Renewable and Sustainable Energy Reviews*, vol. 67, pp. 988–997, jan 2017.

[26] P. Mahat, Z. Chen, B. Bak-Jensen, and C. L. Bak, "A simple adaptive overcurrent protection of distribution systems with distributed generation," *IEEE Transactions on Smart Grid*, vol. 2, pp. 428–437, sep 2011.

[27] A. Oudalov and A. Fidigatti, "Adaptive network protection in microgrids," *ABB International Journal of Distributed Energy Resources*, vol. 5, no. January 2009, pp. 201–227, 2009.

[28] H. F. Habib, M. M. Esfahani, and O. Mohammed, "Development of protection scheme for active distribution systems with penetration of distributed generation," in *SoutheastCon 2018*, vol. 2018-April, pp. 1–7, IEEE, apr 2018.

[29] F. Coffele, C. Booth, and A. Dyśko, "An adaptive overcurrent protection scheme for distribution networks," *IEEE Transactions on Power Delivery*, vol. 30, no. 2, pp. 561–568, 2015.

[30] W. L. Peiris, W. H. Eranga, K. T. Hemapala, and W. D. Prasad, "An adaptive protection scheme for small scale microgrids based on fault current level," *2018 2nd International Conference On Electrical Engineering, EECon 2018*, pp. 64–70, 2018.

[31] E. Sortomme, M. Venkata, and J. Mitra, "Microgrid protection using communication-assisted digital relays," in *IEEE PES General Meeting*, pp. 1–1, 2010.

[32] M. Dewadasa, A. Ghosh, and G. Ledwich, "Protection of microgrids using differential relays," in *AUPEC 2011*, pp. 1–6, 2011.

[33] T. S. Ustun, C. Ozansoy, and A. Zayegh, "Differential protection of microgrids with central protection unit support," in *IEEE 2013 Tencon - Spring*, pp. 15–19, 2013.

[34] E. Sortomme, J. Ren, and S. S. Venkata, "A differential zone protection scheme for microgrids," in *2013 IEEE Power Energy Society General Meeting*, pp. 1–5, 2013.

[35] A. Zidan, M. Khairalla, A. M. Abdrabou, T. Khalifa, K. Shaban, A. Abdrabou, R. El Shatshat, and A. M. Gaouda, "Fault detection, isolation, and service restoration in distribution systems: State-of-the-art and future trends," *IEEE Transactions on Smart Grid*, vol. 8, pp. 2170–2185, sep 2017.

[36] X. Li, A. Dysko, and G. M. Burt, "Traveling wave-based protection scheme for inverter-dominated microgrid using mathematical morphology," *IEEE Transactions on Smart Grid*, vol. 5, no. 5, pp. 2211–2218, 2014.

[37] H. Al-Nasseri, M. Redfern, and F. Li, "A voltage based protection for micro-grids containing power electronic converters," in *2006 IEEE Power Engineering Society General Meeting*, p. 7 pp., IEEE, 2006.

[38] H. Al-Nasseri and M. A. Redfern, "Harmonics content based protection scheme for Micro-grids dominated by solid state converters," in *2008 12th International Middle-East Power System Conference*, pp. 50–56, IEEE, mar 2008.

[39] F. Zhang and L. Mu, "A fault detection method of microgrids with grid-connected inverter interfaced distributed generators based on the PQ control strategy," *IEEE Transactions on Smart Grid*, vol. 10, pp. 4816–4826, sep 2019.

[40] H. Li, G. Rosenwald, J. Jung, and C. C. Liu, "Strategic power infrastructure defense," *Proceedings of the IEEE*, vol. 93, no. 5, pp. 918–933, 2005.

[41] F. Blaabjerg, Y. Yang, D. Yang, and X. Wang, "Distributed power-generation systems and protection," *Proceedings of the IEEE*, vol. 105, no. 7, pp. 1311–1331, 2017.

[42] B. Mohar, Y. Alavi, G. Chartrand, O. Oellermann, and A. Schwenk, "The Laplacian spectrum of graphs," *Graph Theory, Combinatorics and Applications*, vol. 2, p. 5364, 01 1991.

[43] B. Yang, V. Vittal, and G. T. Heydt, "Slow-coherency-based controlled islanding - A demonstration of the approach on the August 14, 2003 blackout scenario," *IEEE Transactions on Power Systems*, vol. 21, no. 4, pp. 1840–1847, 2006.

[44] G. Xu and V. Vittal, "Slow coherency based cutset determination algorithm for large power systems," *IEEE Transactions on Power Systems*, vol. 25, no. 2, pp. 877–884, 2010.

[45] J. Li, C. C. Liu, and K. P. Schneider, "Controlled partitioning of a power network considering real and reactive power balance," *IEEE Transactions on Smart Grid*, vol. 1, pp. 261–269, dec 2010.

[46] L. Che, X. Zhang, M. Shahidehpour, A. Alabdulwahab, and Y. Al-Turki, "Optimal planning of loop-based microgrid topology," *IEEE Transactions on Smart Grid*, vol. 8, no. 4, pp. 1771–1781, 2017.

[47] C. A. Cortes, S. F. Contreras, and M. Shahidehpour, "Microgrid topology planning for enhancing the reliability of active distribution networks," *IEEE Transactions on Smart Grid*, vol. 9, no. 6, pp. 6369–6377, 2018.

[48] I. Schweitzer Engineering Laboratories, "Sel-751 feeder protection relay," 2021.

[49] R. Morello, S. C. Mukhopadhyay, Z. Liu, D. Slomovitz, and S. R. Samantaray, "Advances on sensing technologies for smart cities and power grids: A review," *IEEE Sensors Journal*, vol. 17, no. 23, pp. 7596–7610, 2017.

[50] E. Y. Song, G. J. FitzPatrick, and K. B. Lee, "Smart sensors and standard-based interoperability in smart grids," *IEEE Sensors Journal*, vol. 17, no. 23, pp. 7723–7730, 2017.

[51] Simulink, "Simulation and model-based design," 2020.

[52] DIgSILENT, "DIgSILENT PowerFactory," 2021.

[53] W. Kersting, "Radial distribution test feeders," *IEEE Transactions on Power Systems*, vol. 6, no. 3, pp. 975–985, 1991.

[54] W. Kersting, "Radial distribution test feeders," in *2001 IEEE Power Engineering Society Winter Meeting. Conference Proceedings (Cat. No.01CH37194)*, vol. 2, pp. 908–912 vol.2, 2001.

[55] *Electrical distribution-system protection.* Cooper Industries, 3 ed., 1990.

[56] E. Sortomme, G. J. Mapes, B. A. Foster, and S. S. Venkata, "Fault analysis and protection of a microgrid," in *2008 40th North American Power Symposium*, pp. 1–6, 2008.

[57] D.-P. Cong, B. Raison, J.-P. Rognon, S. Bonnoit, and B. Manjal, "Optimization of fault indicators placement with dispersed generation insertion," in *IEEE Power Engineering Society General Meeting, 2005*, pp. 355–362 Vol. 1, 2005.